Validation of a Water Vapor Micropulse Differential Absorption Lidar (DIAL)

TAMMY M. WECKWERTH AND KRISTY J. WEBER

Earth Observing Laboratory, National Center for Atmospheric Research,[a] *Boulder, Colorado*

DAVID D. TURNER[b]

National Oceanic and Atmospheric Administration/National Severe Storms Laboratory, Norman, Oklahoma

SCOTT M. SPULER

Earth Observing Laboratory, National Center for Atmospheric Research,[a] *Boulder, Colorado*

(Manuscript received 9 June 2016, in final form 22 August 2016)

ABSTRACT

A water vapor micropulse differential absorption lidar (DIAL) instrument was developed collaboratively by the National Center for Atmospheric Research (NCAR) and Montana State University (MSU). This innovative, eye-safe, low-power, diode-laser-based system has demonstrated the ability to obtain unattended continuous observations in both day and night. Data comparisons with well-established water vapor observing systems, including radiosondes, Atmospheric Emitted Radiance Interferometers (AERIs), microwave radiometer profilers (MWRPs), and ground-based global positioning system (GPS) receivers, show excellent agreement. The Pearson's correlation coefficient for the DIAL and radiosondes is consistently greater than 0.6 from 300 m up to 4.5 km AGL at night and up to 3.5 km AGL during the day. The Pearson's correlation coefficient for the DIAL and AERI is greater than 0.6 from 300 m up to 2.25 km at night and from 300 m up to 2.0 km during the day. Further comparison with the continuously operating GPS instrumentation illustrates consistent temporal trends when integrating the DIAL measurements up to 6 km AGL.

1. Introduction

There is a long-standing and certain need for improved atmospheric moisture measurements within and just above the atmospheric boundary layer (BL; defined here to be the lowest 2–3 km above the earth's surface). Several recent National Research Council (NRC) reports highlighted the requirement for improved moisture and wind measurements in the BL as a necessary step toward improving numerical weather prediction (NWP) and quantitative precipitation forecasting (QPF) skill (NRC 2009, 2010, 2012). The highest-priority observational needs within a distributed adaptive nationwide network of networks that would be designed to observe conditions near the earth's surface are high-resolution vertical profiles of humidity in the BL, along with measurements of BL depth, soil moisture and temperature profiles, and air quality (NRC 2009). A subsequent report stated the requirement of obtaining height-resolved moisture measurements in the BL for improving severe weather forecasting skill and for obtaining improved accuracy in QPF skill. This latter report noted that ''moisture and BL wind field observations are likely to be even more important on the mesoscale.'' (NRC 2012, p. 87). Optimal temporal resolution requirements for profiling water vapor ranges from better than 1 h for monitoring purposes to better than 1 min for turbulence studies (e.g., Weckwerth et al. 1999; Turner et al. 2014; Wulfmeyer et al. 2015). The differential absorption lidar (DIAL) validated in this

[a] The National Center for Atmospheric Research is sponsored by the National Science Foundation.

[b] Current affiliation: Global Systems Division, NOAA/Earth System Research Laboratory, Boulder, Colorado.

Corresponding author address: Tammy Weckwerth, Earth Observing Laboratory, National Center for Atmospheric Research, 3450 Mitchell Lane, Boulder, CO 80303.
E-mail: tammy@ucar.edu

DOI: 10.1175/JTECH-D-16-0119.1

paper is proposed as an instrument to partially address the measurement gap in continuous profiling of BL water vapor.

Moisture variations may occur on the 1–2-km horizontal spatial scale, for example, those caused by BL structures, such as horizontal convective rolls (e.g., Weckwerth et al. 1996). These scales of variability are important for describing the atmospheric instability that is essential for the prediction of thunderstorm initiation and severe weather events (e.g., Crook 1996; Weckwerth et al. 1996; Weckwerth 2000; Lin et al. 2011). Forecasters have noted the value of real-time GPS precipitable water vapor (PWV) observations in detecting rapid moisture increases to improve their high-impact weather forecasting skill (e.g., Moore et al. 2015). When humidity profiles from a microwave radiometer profiler (MWRP) and Atmospheric Emitted Radiance Interferometer (AERI; Knuteson et al. 2004a,b) were assimilated, along with temperature and wind profiles, improved QPF timing, location, and intensity skill were achieved (e.g., Hartung et al. 2011; Otkin et al. 2011). Improved forecasting skill in certain conditions was also shown when assimilating water vapor DIAL data (e.g., Wulfmeyer et al. 2006; Harnisch et al. 2011).

Required observations of high temporal and vertical resolution profiles of water vapor in the lower troposphere are difficult to achieve. The standard for water vapor profiling is the radiosonde, providing in situ measurements during its ascent. These soundings are launched operationally worldwide but typically only twice a day (normally at 0000 and 1200 UTC) per site and the sites are separated by hundreds of kilometers. They are often not representative of the mesoscale environment needed for improving forecasts of thunderstorms. Satellite retrievals provide global coverage but have poor vertical resolution and limited temporal resolution. Furthermore, satellites commonly use infrared spectral methods to derive water vapor profiles but clouds, which often occur in dynamic weather conditions, obscure the BL because clouds are usually optically thick in the infrared. Since ground-based MWRPs require periodic manual calibration, systematic biases in the calibration (e.g., Paine et al. 2014) can occur that impact the retrieved thermodynamic profiles (e.g., Löhnert and Maier 2012), and they have only limited information content, resulting in poor vertical resolution (Löhnert et al. 2009). Ground-based infrared radiometers, like the AERI, have higher information content than microwave radiometers (Löhnert et al. 2009), resulting in higher vertical resolution, but they provide only retrieval information in the lowest few kilometers. GPS receivers provide column-integrated PWV without range-resolved height information. With a dense network of GPS receivers, tomographic retrievals can be performed to obtain the three-dimensional moisture field, but the vertical and horizontal resolution is limited by the separation between ground stations (e.g., Van Baelen et al. 2011; Weckwerth et al. 2014). Raman lidars, although capable of providing accurate range-resolved water vapor profiles, require high-power laser transmitters and a large receiver aperture due to the relatively weak Raman scattering signal and thus are currently very expensive (e.g., Turner and Goldsmith 1999). Furthermore, Raman lidars require a calibration technique based on an ancillary measurement for quantitative water vapor retrievals. Nevertheless, Raman lidars are available operationally at four sites to our knowledge: two Atmospheric Radiation Measurement (ARM) sites in Oklahoma and the Azores (Goldsmith et al. 1998; Turner and Goldsmith 1999; Turner et al. 2016a), the Payerne, Switzerland, site (Dinoev et al. 2013), and the Lindenberg, Germany, site (Reichardt et al. 2012). The significant cost to purchase and operate these high-power Raman systems, however, limits their overall use in large networks. DIAL systems offer an alternative active remote sensing measurement of water vapor but place high demands on the properties of the laser transmitter. The DIAL system described herein was developed to utilize lasers based on semiconductor gain media to keep costs low and was designed to simplify and stabilize the system to allow for unattended continuous operations.

In an effort to gain confidence in this DIAL and to characterize its operating strengths and limitations, this manuscript will show comparisons with multiple other ground-based water vapor sensing instruments, described in section 2. Comparison techniques will follow those developed by Behrendt et al. (2007), Bhawar et al. (2011), and Turner and Löhnert (2014), and will also be described in section 2. The comparison results will be shown in section 3 followed by the summary and outlook in section 4.

2. Instruments and methodology

Data to be compared with the DIAL were collected during two field projects in different locations: The Front Range Air Pollution and Photochemistry Experiment (FRAPPÉ; Flocke et al. 2015) occurred 1 July–15 August 2014 in a relatively dry environment in Erie, Colorado; and the Plains Elevated Convection at Night (PECAN; Ellis, Kansas; Geerts et al. 2016) field campaign was conducted 1 June–15 July 2015 in a relatively humid environment in Hays, Kansas.

a. DIAL

This eye-safe water vapor micropulse DIAL (Spuler et al. 2015) is a low-power active remote sensing system

TABLE 1. Specifications of DIAL during FRAPPÉ and PECAN.

DIAL transmitter	
Seed laser	Two DBR lasers
Amplifier	Single-stage TSOA
Pulse energy	5 μJ
Pulse duration	1 μs (150 m)
PRF	9 kHz (FRAPPÉ); 7 kHz (PECAN)
Wavelength	828.198–828.1990 nm (online FRAPPÉ) 828.2974–828.2985 nm (offline FRAPPÉ) 828.2000 nm (online PECAN) 828.2995 nm (offline PECAN)
Beam divergence	70 μrad
DIAL receiver	
Telescope	40.6-cm-diameter f/3 Newtonian
Field of view	120 μrad (narrow FOV) 450 μrad (wide FOV in FRAPPÉ) 300 μrad (wide FOV in PECAN)
Effective far-field bandpass	0.14 nm
Averaging time	1–25 min
Sampling rate	0.5 μs (75 m)

that was significantly upgraded from preceding generations of prototypes developed and tested at Montana State University (MSU; Nehrir et al. 2009, 2011, Nehrir 2011; Nehrir et al. 2012; Repasky et al. 2013). Water vapor DIALs based on more powerful solid-state laser transmitters, that similarly sample the lower troposphere, have been fielded successfully as both ground-based (e.g., Wulfmeyer and Bösenberg 1998; Vogelmann and Trickl 2008; Behrendt et al. 2009; Wagner et al. 2013; Späth et al. 2016) and airborne systems (e.g., Ehret et al. 1993; Browell et al. 1997; Bruneau et al. 2001; Poberaj et al. 2002). However, none of these high-power systems was designed to run operationally in an unattended mode.

The transmitter for this relatively small state-of-the-art micropulse DIAL system uses a diode laser following prior advances by Machol et al. (2004). The current instrument uses a pulsed laser transmitter that can produce two wavelengths around 828 nm (Table 1) via two distributed Bragg reflector (DBR) diode lasers that injection seed a tapered semiconductor optical amplifier (TSOA). The elapsed time between transmitting and receiving the backscattered laser pulse is used to determine range information. The online wavelength is tuned near the center of the water vapor absorption line, and the second transmitted wavelength is chosen such that it is minimally affected by the atmospheric water vapor. A fast 100-Hz switching frequency between the online and offline wavelengths allows for measurements in strong vertical and temporal gradient regions. Atmospheric aerosols provide the majority of the backscattered signal, as Rayleigh (i.e., molecular) scattering is relatively weak at the 828-nm laser wavelengths. Eye safety is achieved at the exit port due to beam expansion through a shared Newtonian telescope design.

The Newtonian telescope is also used as the receiver to collect the backscattered light, which is then directed through a narrowband filter and a Fabry–Perot etalon with a free spectral range of 0.1 nm equal to the wavelength difference between the online and offline signals. Most of the backscattered light (90%) is directed through a second narrowband filter and then to a fiber-coupled avalanche photodiode. The remaining 10% of the reflected light is used for a wide field-of-view (FOV) measurement via a second receiver channel (Spuler et al. 2015).

The ratio of the return power between the online and offline signals, and knowledge of the molecular absorption cross section, are used to determine the range-resolved water vapor number density, or absolute humidity. Since the ratio of backscattered powers from closely spaced transmitted DIAL wavelengths ($\Delta\lambda = 0.1$ nm) is used to determine the water vapor, the differential attenuation in the two channels due to extinction by molecules and aerosol particles is negligible, and therefore no external calibration procedures are necessary (e.g., Ismail and Browell 1989). Furthermore, having a single detector for both wavelengths eliminates the need to account for the instrument overlap function that tends to be a problem for Raman lidars.

The laser pulse length and eventually the overlap function limit the minimum range of the DIAL. The detector is temporarily blinded by the transmitted pulse and cannot measure the backscattered signal until the pulse has fully exited the transceiver. As configured for FRAPPÉ and PECAN, the instrument's minimum range gate was 300 m. Future modifications to sample lower to the earth's surface are discussed in the conclusions.

The primary errors for a low-power micropulse DIAL are explained in Spuler et al. (2015); these photon-counting systems are dominated by solar background error during daytime operation and by Poisson error during nighttime. Speckle error is another but smaller error term that should be considered in a complete analysis (Wulfmeyer and Walther 2001a,b). An additional error term, and one that is more difficult to quantify, comes from Rayleigh–Doppler (RD) broadening of the laser light when backscattered by molecules (Ansmann and Bösenberg 1987). The narrowband DIAL equation, as shown in Spuler et al. (2015), assumes negligible broadening from backscatter that is appropriate for one-way transmission and aerosol backscatter. However, the absorption coefficient in the backscattered direction must be corrected for the broadband molecular backscatter contribution. A DIAL instrument may require RD corrections in regions where scattering is predominately from molecules (e.g., in aerosol-free regions aloft) and in regions with strong backscatter gradients (e.g., cloud edges). The DIAL system described herein was designed to minimize the RD error through the use of an ultra-narrowband filter that blocks approximately half of the spectrally broadened molecular return. Additionally, the instrument operates on the side of a water vapor absorption line that further reduces the sensitivity to RD error (Späth et al. 2016). Regions of high gradients, such as cloud edges, were masked out, and it is expected that RD errors in the remaining regions are typically below 5% based on model results. Therefore, no RD corrections were applied for the dataset analyzed herein. NCAR is investigating incorporating a high spectral resolution lidar (HSRL) channel at 780 nm (Hayman et al. 2015) into the instrument that would measure the aerosol-to-molecular backscatter ratio and allow for accurate RD corrections in the future.

In addition to the systematic errors mentioned above, there can be errors due to instrument misalignment. A small misalignment of the angle of the narrowband interference filter used to reduce the solar background will more severely affect those signals coming from the near range (below 750 m) because the divergence of these signals is largest. For this DIAL, a wide FOV channel was implemented to avoid angle-induced errors associated with the daylight filter—the path does not contain the most angle-sensitive narrowband filter stage. To minimize angular errors, the wide channel return is used as feedback to align the main channel and produce quality data at low ranges with excellent solar background suppression. The wide channel will have varying day/night performance due to the larger field of view and the lack of one filtering stage, and it is not useful as a daytime data product; therefore, it is used for alignment only and is not used for data analysis.

One of the most significant upgrades to the earlier version of the water vapor DIAL developed by MSU is the ability to obtain continuous unattended moisture profiles (Spuler et al. 2015). Figure 1 shows the continuous data collected by the DIAL for 51 days each for FRAPPÉ (UCAR/NCAR EOL 2016b) and PECAN (UCAR/NCAR EOL 2016a). Water vapor and attenuated backscatter profiles were averaged and compiled with 30-s resolution and are plotted as 5-min averages. The DIAL's vertical grid spacing used in the subsequent comparisons is 75 m because that is the sampling rate of the instrument. Figures 1a,c illustrate the relative aerosol backscatter from 300 m up to 12 km, while Figs. 1b,d illustrate the water vapor absolute humidity profiles from 300 m up to 6 km AGL. Vertical white strips from the ground to the top of the panel indicate missing data due to maintenance or other down periods. Note the continuity of both time series illustrating that the DIAL was operational more than 95% of the time for both FRAPPÉ and PECAN, shutting down only sporadically due to the experimental instrument control software. The yellow/red regions of relative backscatter illustrate cloud bases. Water vapor measurements via the DIAL are not possible through optically thick clouds, and these regions are displayed as white for missing data segments.

The depth of the BL as shown by the relatively high aerosol backscatter intensity near the ground was greater in Colorado during FRAPPÉ than in Kansas during PECAN. This higher aerosol content in FRAPPÉ allowed for stronger signal strength and contributed to the maximum height of the water vapor retrieval being greater in Colorado. The water vapor content was lower in Colorado, consistent with the relatively lower humidity in the region. This relatively low moisture content was another contributor to the greater height range of the water vapor retrieval in Colorado because the DIAL was tuned to the wing of the water vapor absorption line during FRAPPÉ, which allowed for better detection of the lower moisture values aloft. The water vapor profiles show diurnal variability in both water vapor amount and depth of the moisture layer near the ground. The range of the water vapor signal is limited because the water vapor density and hence signal strength decrease with height. The moisture profiles extend to greater heights at night than during the day due to the difficulty in filtering out the strong daytime background solar radiation.

b. *Radiosondes*

The radiosonde data were recorded every 1 s, which corresponded to a vertical resolution of 4–6 m. Since the radiosonde vertical resolution was better than the DIAL resolution, the radiosonde data were averaged into 75-m bins to compare with the DIAL data. The DIAL data

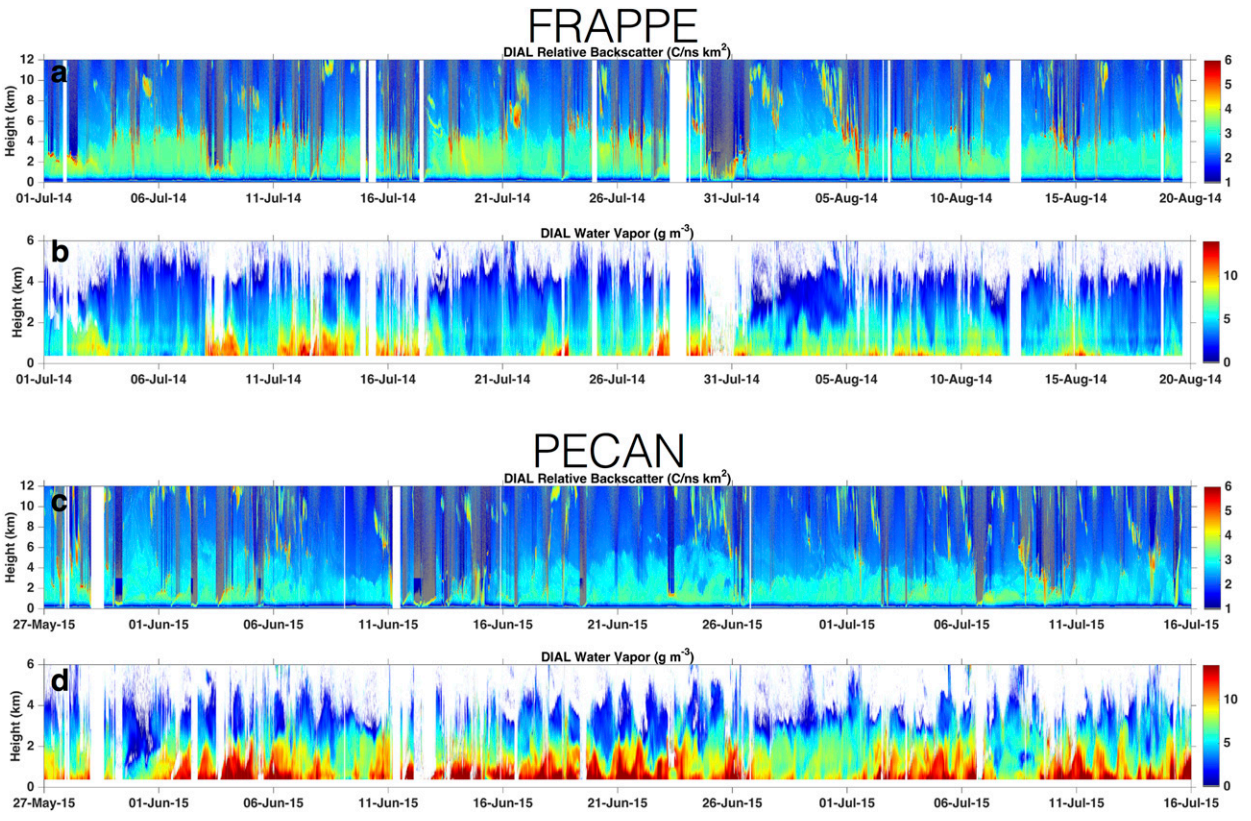

FIG. 1. Time series of decimated 5-min/75-m DIAL profiles at (a),(b) FRAPPÉ and (c),(d) PECAN showing (a),(c) range-corrected relative backscatter and (b),(d) absolute humidity (g m^{-3}). Vertical white bars signify missing data due to DIAL downtime or attenuated signal above optically thick clouds.

were averaged for 5 min starting at the radiosonde launch time to allow the radiosonde to ascent to ~1.5 km AGL during the comparison period.

The radiosonde observations of relative humidity, temperature, and pressure are converted to absolute humidity (ρ_{WV}) for comparison with the DIAL ρ_{WV} direct observations. Table 2 shows the number of radiosondes used in these comparisons. All 33 of the FRAPPÉ soundings except one were launched around noon local time. Midday is the most difficult time for a DIAL because the solar background radiation is close to its maximum intensity, resulting in a lower signal-to-noise ratio than experienced at other times of the day. Of the 133 PECAN radiosondes (Clark 2016), only 39 were launched during the daytime (0630–2100 CDT) due to the nighttime focus of the PECAN experiment.

During FRAPPÉ the radiosondes were Vaisala RS92s and were corrected for dry bias caused by solar radiative heating of the relative humidity sensor arm following Wang et al. (2013). The sounding launch site was collocated with the DIAL and AERI. During PECAN the radiosondes were Vaisala RS41s, which do not require dry bias correction due to the improved design that minimizes radiation effects. The PECAN sounding launch site was 2.1 km south of the DIAL/AERI/MWRP/GPS location.

The radiosondes are advected by the wind as they ascend, while the remote sensors provide profile information directly above the instruments. This could

TABLE 2. Number of profiles used in plots and statistical comparisons. Number in parentheses shows the percentage of available profiles removed from analyses due to dissimilar profiles. See text for explanation of how and why dissimilar profiles were removed from DIAL comparisons with AERI and MWRP.

FRAPPÉ	
DIAL–radiosondes	33 (0)
Daytime DIAL–AERI	1870 (17)
Nighttime DIAL–AERI	2581 (13)
PECAN	
Daytime DIAL–radiosondes	39 (0)
Nighttime DIAL–radiosondes	94 (0)
Daytime DIAL–AERI	4582 (28)
Nighttime DIAL–AERI	3993 (19)
Daytime DIAL–MWRP	4036 (32)
Nighttime DIAL–MWRP	3491 (25)

provide a source of discrepancy in the DIAL–radiosonde comparisons. To correct for this possible discrepancy between the DIAL and radiosondes, Lagrangian back-trajectory calculations were applied to account for the horizontal displacement of the radiosonde during its ascent. The uncorrected sounding results compared as favorably as the corrected results; thus, the comparisons shown herein will use the actual radiosonde data without any horizontal displacement corrections applied.

c. AERI

The AERI is an operational passive remote sensing system that was designed at the University of Wisconsin–Madison for the ARM Program (Stokes and Schwartz 1994; Turner et al. 2016b). The AERI measures downwelling infrared radiance at approximately $1\,\mathrm{cm}^{-1}$ resolution from 520 to $3000\,\mathrm{cm}^{-1}$ (i.e., 19.2–3.3 μm; Knuteson et al. 2004a). Accurate radiance measurements are obtained through the use of two well-characterized National Institute of Standards and Technology (NIST)-traceable blackbodies that are viewed every 3 min (Knuteson et al. 2004b). The temporal resolution of the radiance observations is 20 s, and a principal component–based noise filter is used to greatly reduce the random error in the observations (Turner et al. 2006). The retrieval of temperature and water vapor profiles, as well as cloud properties, is possible via the principle that channels that are close to the center of the absorption lines are more opaque and thus more sensitive to low altitudes, while channels away from the center of the absorption lines are more transparent and can thus provide information from higher altitudes (Wulfmeyer et al. 2015). The AERI retrieval algorithm used in this analysis is the advanced optimal estimation (AERIoe) technique described in Turner and Löhnert (2014); this algorithm provides a full error characterization of each retrieval and the information content in the AERI radiance observations. This approach can also retrieve thermodynamic profiles from the AERI radiance data in cloudy scenes, although the AERI observations have virtually no information on the structure of the profile above cloud base.

In previous comparisons within clear skies below 2 km, where the AERI retrievals provide the most information, AERI-observed mixing ratio profiles are within $0.3\,\mathrm{g\,kg}^{-1}$ of radiosonde profiles with the RMS error being less than $1.2\,\mathrm{g\,kg}^{-1}$ (Blumberg et al. 2015). The vertical resolution of the retrieved water vapor profiles from the AERI is ~50, 800, 1200, and 2500 m at 300 m, 1 km, 2 km, and 3 km AGL, respectively. The vertical resolution of the AERIoe retrievals is determined by two factors: 1) the infrared weighting functions and 2) the level-to-level correlation in the a priori dataset used to constrain the retrieval. These two factors are combined in the averaging kernel. Turner and Löhnert (2014) describe how the vertical resolution is derived from the averaging kernel and provide an illustration of the typical vertical resolution as a function of height. Importantly, however, the first-guess profile has no influence on the vertical resolution of the retrieved profile. AERI data are used herein only up to 3 km, as there is virtually no information about the humidity profile in the AERI radiance observation above that height (Löhnert et al. 2009).

An AERI from University of Wisconsin–Madison was fielded next to the DIAL and radiosonde launch site in Erie for FRAPPÉ and an AERI instrument from the DOE ARM Program (Turner and Ellingson 2016) was collocated with the DIAL in Ellis for PECAN. The AERI-retrieved temperature profiles were used together with the AERI-retrieved water vapor mixing ratio data in order to derive absolute humidity for the statistical comparisons with the DIAL (Turner 2015). The DIAL and AERI absolute humidity datasets were compared using 5-min and 75-m temporal and spatial resolution, respectively, over the depth of 300 m–3 km AGL. This averaging was chosen to preserve small-scale variability but reduce substantial noise and to match the DIAL height bins. If there was no data point in the same height range being matched to the DIAL, then AERI was assigned a ''no data'' value and that point was not compared.

d. MWRP

MWRPs are mature passive remote sensing systems that are operated continuously within networks (e.g., Crewell et al. 2004; Cimini et al. 2012; Cadeddu et al. 2013; Illingworth et al. 2015). A Radiometrics MP3000 was fielded by the University of Manitoba and was collocated with the DIAL and AERI during PECAN. Similar to the AERI, the observed radiation is sensitive to the temperature and water vapor profiles from all heights in the column above the radiometer and the range information is available after retrieval algorithms are applied, which account for the different signal strengths at different wavelengths. Calibration methods are more difficult with the MWRPs than with AERIs, requiring the use of periodic viewing of an external calibration source (Maschwitz et al. 2013; Küchler et al. 2016). MWRPs have less information content and thus provide lower vertical resolution than AERIs (Löhnert et al. 2009; Blumberg et al. 2015). However, unlike the AERI, MWRPs have some information above cloud base in cloudy conditions due to the lower opacity of clouds at microwave wavelengths relative to infrared wavelengths.

The analyses and comparisons herein use the retrieval produced by the Radiometerics operational algorithm, which is a neural network (NN)-based statistical retrieval (Solheim et al. 1998). While the vertical grid spacing used in the NN algorithm is 50 m up to 0.5 km, 100 m up to 2 km and 250 m above 2 km the true vertical resolution is ~1500, 2400, 2700, and 4000 m at 300 m, 1 km, 2 km, and 3 km AGL, respectively (Blumberg et al. 2015). The vertical resolution of the MWRP is controlled by the same factors as the AERI; however, the weighting functions in the microwave are fewer and less peaked, resulting in a vertical resolution that is coarser than the AERI's. Note that various studies have shown that one-dimensional variational retrieval approaches (such as the optimal estimation approach used for the AERI) provide more accurate results than the NN method (e.g., Cimini et al. 2006; Hewison 2007). Using a NN method, Liljegren (2004) showed a bias of 0.5 g m^{-3} and a standard deviation of 1.5 g m^{-3} compared with radiosondes, whereas a physical retrieval using the same optimal estimation framework as the AERI demonstrated a bias between the MWRP and radiosonde profile of 0.5 g kg^{-1}, an RMS difference of 1.3 g kg^{-1}, and a significantly larger RMS difference than the AERI in the lowest 2 km (Blumberg et al. 2015). However, the standard NN retrieval was used herein because that is available operationally.

The DIAL–MWRP comparisons were made with 75-m and 5-min averages. Similar to the AERI comparisons, DIAL–MWRP comparisons are made only up to 3 km, where the MWRP moisture retrievals are most dependable. MWRP retrievals (Hanesiak and Turner 2015) were available at the DIAL site only during PECAN, as there was not an MWRP deployed during FRAPPÉ.

e. *GPS receivers*

Global Navigation Satellite System (GNSS) signals are received by ground-based GPS receivers. Microwave signals transmitted by satellites are delayed due to atmospheric water vapor as the signals propagate to ground-based GPS receivers. The GPS total delay is closely related to the integrated water vapor along the signal path. The information obtained from ground-based GPS receivers via multiple paths to multiple satellites is combined to derive integrated PWV amounts in the column directly above the GPS receiver (e.g., Bevis et al. 1992, 1994; Businger et al. 1996). The PWV measurement represents a 10–15-km-diameter area centered over the GPS receiver.

A GNSS ground-based GPS receiver was located 12 km northeast of the DIAL/AERI/radiosonde site for FRAPPÉ and was collocated with the DIAL and AERI for PECAN. Recall that the PECAN radiosonde site was 2.1 km south of the other instruments. The GPS data were processed every 30 min, archived, and displayed on the SuomiNet real-time website.

The bias in integrated PWV compared with radiosondes is less than 1 mm with an overall error of less than 5% (Wulfmeyer et al. 2015). The PWV values are processed as 30-min averages. Time series comparisons will be shown as 12-h averages to illustrate comparable trends and to show the value obtained in observations from different height ranges.

3. Comparisons

Comparisons between the DIAL and the other instruments will illustrate the capabilities and operating limitations of the DIAL. Statistical analyses will be shown using scatterplots, profiles of correlation coefficients, mean percentage differences, and standard deviation box-and-whisker plots for point-by-point comparisons between DIAL and other instruments.

While point-by-point comparison statistics are useful for comparing the height range of good agreement between the DIAL and other sensors, Turner and Löhnert (2014) introduced modified Taylor plots (Taylor 2001) to investigate profile-by-profile comparisons. This is done by plotting the modified Pearson's correlation coefficient (r) and the standard deviation ratio (SDR) between the DIAL and the radiosonde for each profile, where

$$r = \frac{\sum(X - \overline{X})(Y - \overline{Y})}{\sqrt{\sum(X - \overline{X})^2}\sqrt{\sum(Y - \overline{Y})^2}},$$

where X is the other instrument's data point and Y is the DIAL data point. The respective overbars are the averages over the vertical range compared. The r value is used in these comparisons as a measure of the linear correlation, ranging from −1 to 1, between the DIAL absolute humidity and the other instrument's absolute humidity, where 1 is a total positive correlation. The SDR is the ratio of the standard deviation of the DIAL absolute humidity values within each 5-min profile versus the standard deviation of the other instrument's absolute humidity values within each 5-min profile.

The PWV time series will be obtained by calculating PWV using different height ranges of DIAL and AERI observations. This will be compared with GPS total column PWV values and the PWV calculated from the full radiosonde ascent.

Continuous vertical water vapor profiles on 22 June 2015 obtained from collocated DIAL, AERI, and MWRP instruments during PECAN are shown in Fig. 2. All three systems provide comparable qualitative water

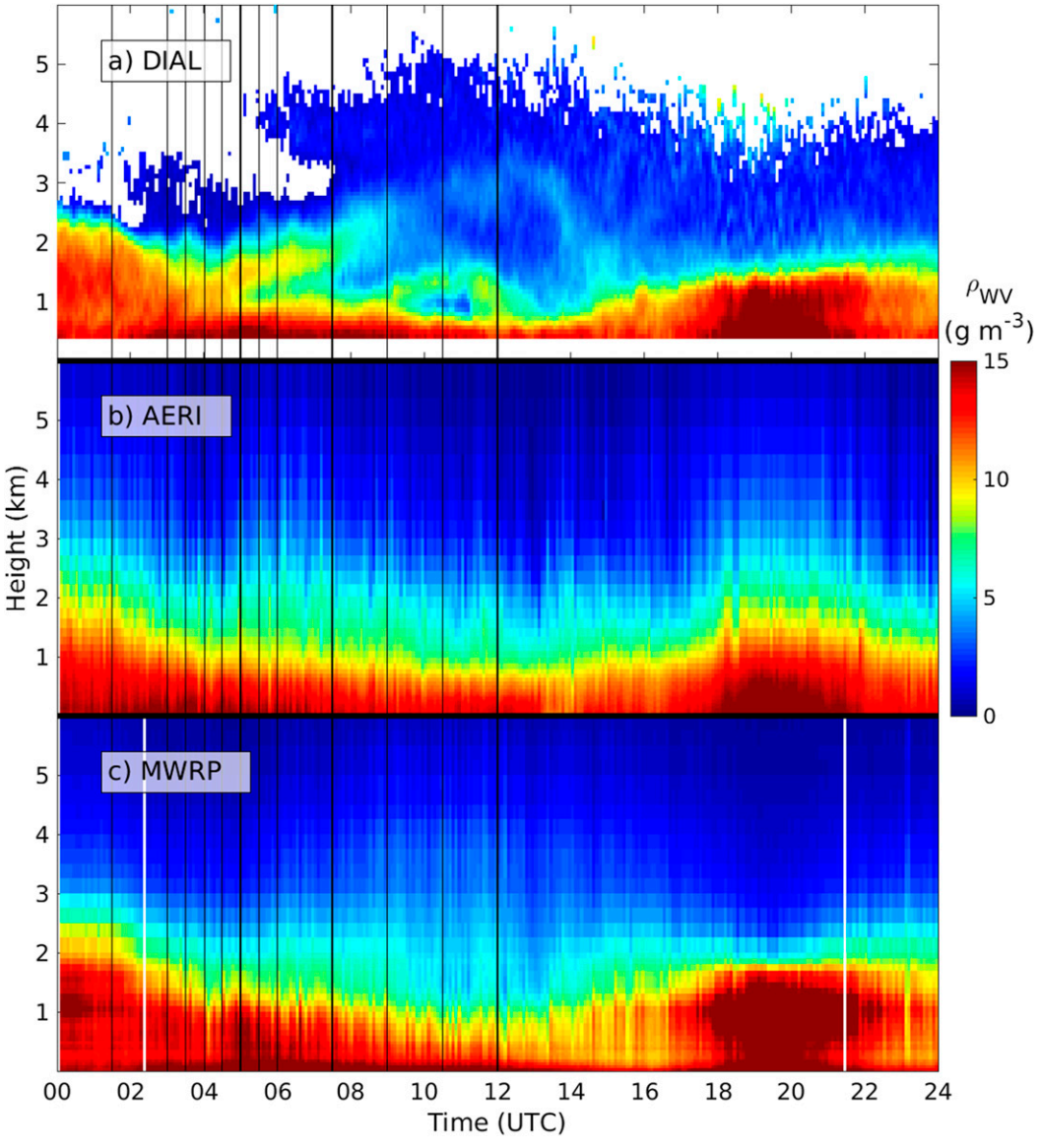

FIG. 2. Absolute humidity (g m^{-3}) time series from (a) DIAL 300 m–6 km AGL, (b) AERI 0–6 km AGL, and (c) MWRP 0–6 km AGL on 22 Jun 2015 during PECAN. Vertical lines indicate times of DIAL and radiosonde comparisons to be shown in Fig. 3.

vapor information, showing decreasing moisture depth from 0000 to 0600 UTC [central daylight time (CDT) = UTC − 5 h during PECAN], minimum moisture depth from 1000 to 1400 UTC, and a moisture maximum at 2000 UTC. It is striking that the DIAL is the only one of these three continuously profiling instruments that can detect the two elevated moist layers from 1 to 3 km AGL during the period ranging from 0600 to 1500 UTC. These elevated moist layers are verified by 12 collocated radiosonde launches from 0500 to 1200 UTC, whose measurements closely match the DIAL observations in both height and absolute humidity values (Fig. 3). The horizontal bars plotted at each 75-m range gate represent the DIAL random relative error estimates, given by Eq. (5) in Spuler et al. (2015). While there are some biases in these detailed comparisons, using 75-m DIAL and 4–6-m radiosonde gates averaged over 5 min starting at the radiosonde launch time, the profiles from the two instruments agree extremely well. In particular, two elevated moist layers at 1.2 and 2.7 km AGL are apparent at 1030 UTC (Fig. 3k). Dry layers are also well verified, such as at 1.2 and 3.2 km AGL at 0730 UTC (Fig. 3i). The standard AERI and MWRP retrievals specify that most of the moisture is at low levels and that

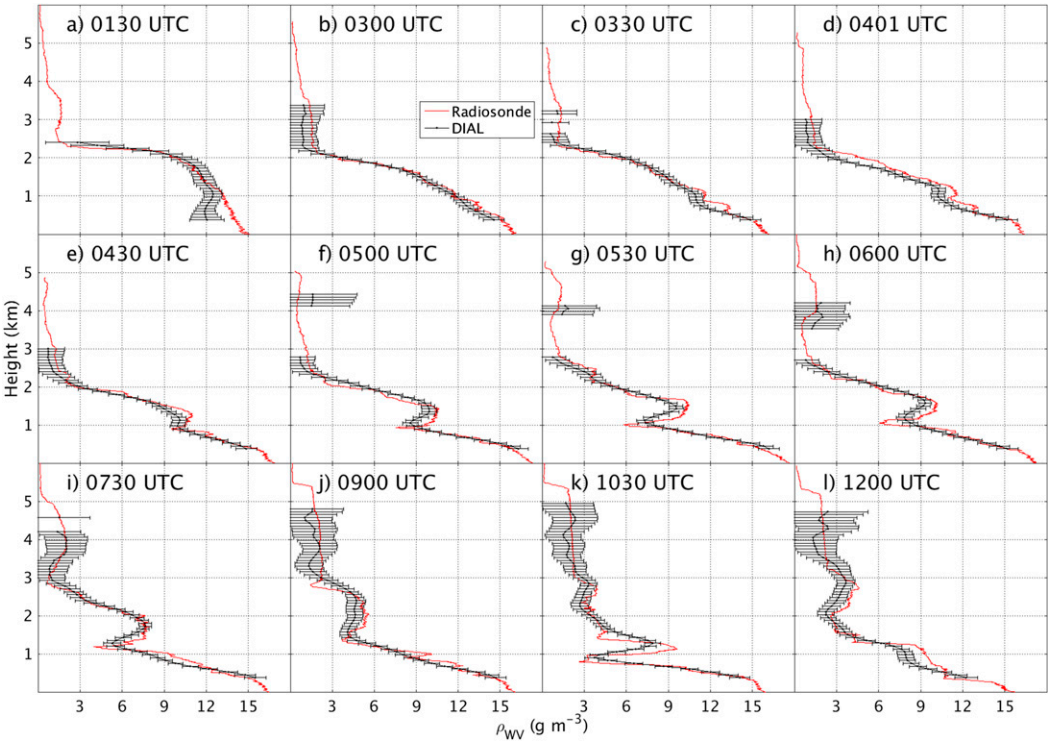

FIG. 3. The 22 Jun 2015 comparisons of DIAL (black lines) and radiosonde (red) absolute humidity profiles (g m^{-3}) at radiosonde launch times of (a) 0130, (b) 0300, (c) 0330, (d) 0401, (e) 0430, (f) 0500, (g) 0530, (h) 0600, (i) 0730, (j) 0900, (k) 1030, and (l) 1200 UTC. Horizontal black lines represent DIAL measurement error at each 75-m height interval. Full-resolution data (DIAL: 75 m; radiosonde: 4–6 m) are plotted. DIAL data are averaged over 5 min starting at the radiosonde launch time.

their vertical resolution decreases sharply with height; therefore, they cannot readily account for elevated moist layers. Such layers are important for monitoring BL evolution, entrainment studies, and atmospheric stability estimates. Compared with the passive remote sensors, the active DIAL has better vertical resolution and better detection capabilities within and atop the BL.

Since the AERI and MWRP instruments cannot detect elevated moist layers, the DIAL profiles with positive gradients are filtered out for the quantitative comparisons with AERI and MWRP discussed in the next section. The profiles with elevated moist layers were identified by adding the number of points in each DIAL profile that had a positive vertical gradient between 300 m and 3 km. If that number of points was greater than 6, the 50th percentile of the summed gradients for each of the campaigns, then the profiles were determined to be dissimilar and were filtered out of the DIAL–AERI and DIAL–MWRP comparisons.

Table 2 shows the number of profiles used for all of the subsequent comparison figures and statistics. The percentage of dissimilar profiles eliminated for each DIAL comparison combination is shown in parentheses. All radiosonde profiles are used in the comparisons, but the dissimilar profiling filter removes many profiles from the comparisons with the passive sensors. More elevated moist layers with positive vertical gradients occurred during PECAN than FRAPPÉ. Furthermore, the mean positive vertical water vapor gradients (not shown) that were detected by the DIAL and filtered out for the intercomparisons were greater for PECAN (0.35 g m^{-3} per 75 m) than for FRAPPÉ (0.21 g m^{-3} per 75 m). The daytime profiles more frequently exhibit elevated moist layers than the nighttime profiles, suggesting that the daytime differential heating may contribute to vertical moisture variability.

a. Correlations between DIAL and other instruments

The scatterplot data points comparing the DIAL and radiosonde points shown in Figs. 4a,b are obtained between 300 m and 6 km. They predominantly follow the one-to-one line with a few outliers at low radiosonde moisture values that have a large range of DIAL moisture values. This is due to residual cloud-edge data points that were not completely masked out during the DIAL signal processing step and/or low signal-to-noise ratio DIAL returns at higher altitudes. For FRAPPÉ, the DIAL–radiosonde comparisons from 300 m to 3 km

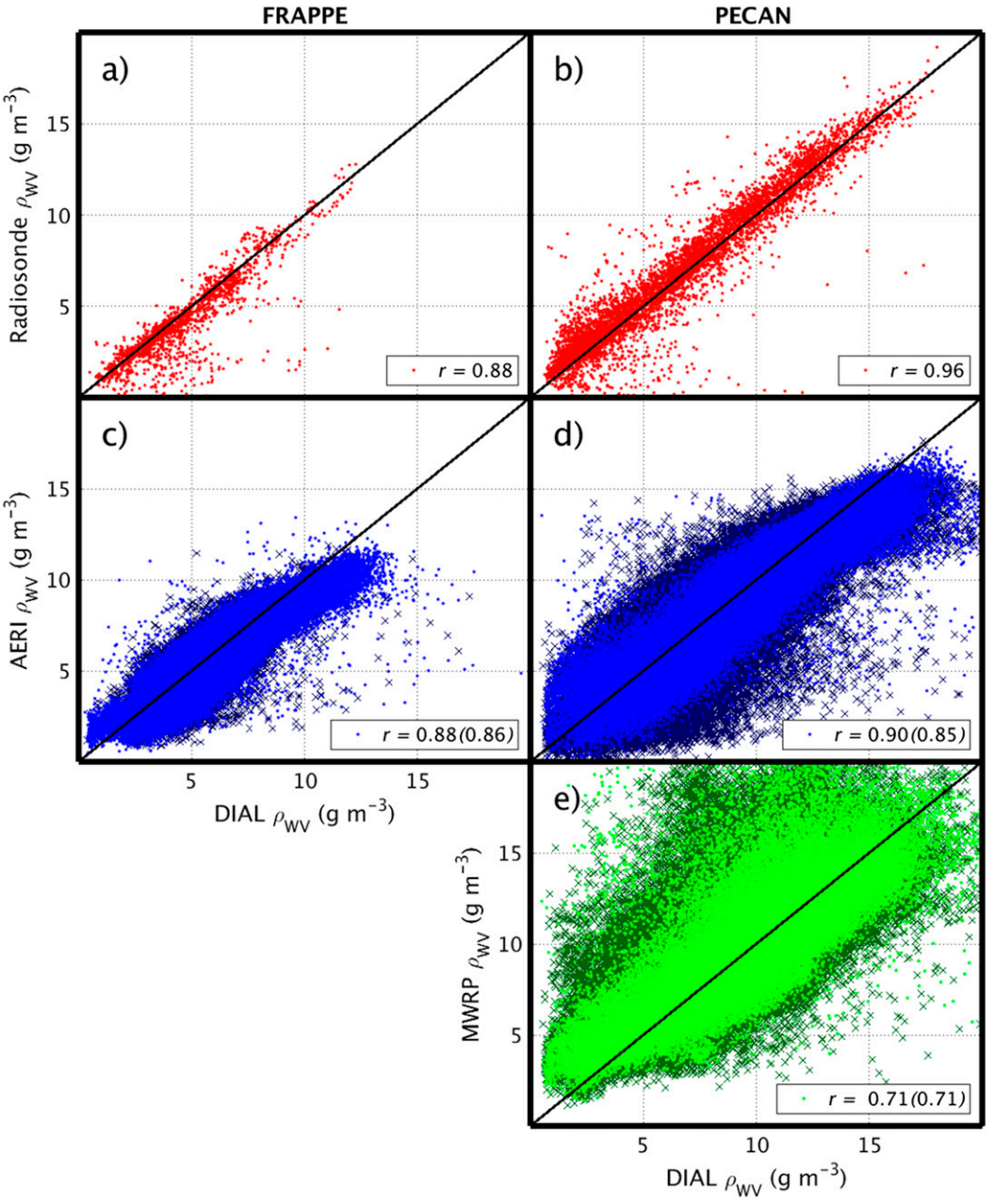

FIG. 4. Scatterplots of absolute humidity (g m^{-3}) from DIAL vs (a),(b) radiosondes compared for 300 m–6 km AGL, (c),(d) AERI compared for 300 m–3 km AGL, and (e) MWRP compared for 300 m–3 km AGL for (left) FRAPPÉ and (right) PECAN. Pearson's *r* is shown for each comparison with *r* in parentheses for dissimilar profile comparisons. (c)–(e) Bright colors near the one-to-one line illustrate comparisons with similar profiles, while dark x's illustrate comparisons with dissimilar profiles exhibiting elevated moist layers (see text for explanation).

(300 m–6 km) have an *r* value of 0.92 (0.88), while for PECAN, *r* is 0.97 (0.96); for the combined dataset, the *r* value is 0.96 (0.95).

Figures 4c,d illustrate the scatterplots of DIAL versus AERI with the similar profile comparisons shown as bright blue dots. The comparisons using dissimilar profiles, defined as containing elevated DIAL moist layers, are shown as dark x's. There are substantially more data points than the DIAL–radiosonde comparisons due to the continuous operations of both DIAL and AERI (also shown in Table 2). It is again clear that PECAN in Kansas exhibited higher water vapor content than FRAPPÉ in Colorado. Excellent agreement (r = 0.88 for FRAPPÉ and r = 0.90 for PECAN) between the

active DIAL and passive AERI are shown in the comparisons for points between 300 m and 3 km AGL. There is significant scatter when using all profiles but the correlations are still high ($r = 0.86$ for FRAPPÉ and $r = 0.85$ for PECAN). There is some scatter even when comparing similar profiles, with the DIAL showing more moisture than the AERI, particularly for high moisture values ($>15\,g\,m^{-3}$), where the AERIoe retrieval has a dry bias. This is likely caused by saturation of the spectral region that provides sensitivity to the AERI water vapor profile (538–588 cm^{-1} in the region). This occurs only in high moisture cases within the AERIoe retrieval (Turner and Löhnert 2014).

The scatterplot in Fig. 4e shows substantially more scatter in the DIAL–MWRP comparisons for both similar (bright green dots) and dissimilar profiles (dark green x's) than the DIAL comparisons with radiosondes (Figs. 4a,b) and AERI (Figs. 4c,d), but it still produces a high r value of 0.71. Similar to the DIAL–AERI comparisons, these point-by-point DIAL–MWRP comparisons are obtained from 300 m to 3 km. Figure 4e suggests that the MWRP retrieval has a moist bias at lower water vapor amounts ($<5\,g\,m^{-3}$), which predominately occur above the BL.

b. Vertical profiles of comparisons

Vertical profiles of r for all comparisons are shown in Fig. 5. For the DIAL–radiosonde daytime comparisons, the FRAPPÉ r value is 0.91 at 300 m AGL and it remains greater than 0.9 (0.6) up to 2.0 (3.5) km AGL (Fig. 5a). Since PECAN had both daytime and nighttime radiosonde launches, comparisons in DIAL data quality for both are shown (Fig. 5b). PECAN daytime results are similar to those of FRAPPÉ. The nighttime DIAL performance at PECAN is better than daytime, as expected, and exhibits $r > 0.60$ up to ~4.5 km AGL.

For the FRAPPÉ DIAL–AERI comparisons, $r > 0.8$ in the first 1 km AGL and $r > 0.6$ up to 2.5 km AGL both day and night (Fig. 5c). The FRAPPÉ profiles show fairly consistent daytime and nighttime comparisons. The PECAN r profiles (Fig. 5d) show $r > 0.6$ up to 2.25 km AGL at night and up to 2.0 km AGL during the day. Since there is no day/night advantage to the AERI retrievals, the better correlation at night is due to the improved DIAL performance at night. The reason that the strong correlations drop off more rapidly during PECAN than FRAPPÉ may be explained by the fact that there is higher water vapor content in Kansas during PECAN than in Colorado during FRAPPÉ (Figs. 1, 4). As Turner and Löhnert (2014) showed, some of the spectral regions used in the AERI retrieval become opaque for more moist air and the information content of the AERI observations is reduced. This results in the degrees of freedom of the AERI retrieval decreasing with increasing water vapor. This loss of AERI information content may be responsible for the DIAL–AERI comparisons being slightly better in FRAPPÉ's environment with lower atmospheric water vapor content.

The correlations between the DIAL and MWRP (Fig. 5e) are substantially lower than the DIAL–radiosondes and DIAL–AERI correlations. It also appears that the nighttime comparison of DIAL–MWRP is worse than the daytime comparison, which is opposite of that expected because MWRP does not have a day/night bias and DIAL performance is better at night. This may be explained by the fact that the MWRP neural network retrieval is trained with radiosondes from the climatological 0000 and 1200 UTC launch times, so it may not be able to determine the differences in the shape of the profiles of day versus night. Additionally, this reduced quality of DIAL–MWRP comparisons may simply illustrate a limitation of the MWRP statistical retrieval method in general.

c. Differences and standard deviations

The mean percent difference (MPD, which is the same as bias if the "truth" is known) is determined by comparing DIAL with all of the other instruments (i.e., radiosondes, AERI and MWRP), written as

$$\mathrm{MPD} = \frac{\sum_{i=1}^{n}\left(\dfrac{\rho_{\mathrm{WV\_DIAL}} - \rho_{\mathrm{WV\_other}}}{\frac{1}{2}(\rho_{\mathrm{WV\_DIAL}} + \rho_{\mathrm{WV\_other}})}\right)}{n} \times 100\%,$$

where $\rho_{\mathrm{WV\_DIAL}}$ is the DIAL water vapor absolute humidity; $\rho_{\mathrm{WV\_other}}$ is radiosonde, AERI, or MWRP absolute humidity; and n is the number of data points within each 250-m height interval. Height bins with <30 comparison points are removed from the plots and statistics.

Box plots of the DIAL observations compared with FRAPPÉ and PECAN radiosondes are shown in Figs. 6a,b. The colored horizontal lines are the MPDs for each 250-m height bin. The boxes represent the 25th–75th percentiles of the differences, and the whiskers represent plus/minus one standard deviation from the mean within each height bin. The FRAPPÉ comparisons between DIAL and radiosondes (Fig. 6a) show excellent agreement with <3% mean difference up to 1.25 km and with good agreement (<10% differences) and little scatter (<20% standard deviations) in the comparisons from 300 m to 2.0 km. This corresponds to the height range of high daytime r values (Fig. 5a). The DIAL absolute humidity values are slightly higher than

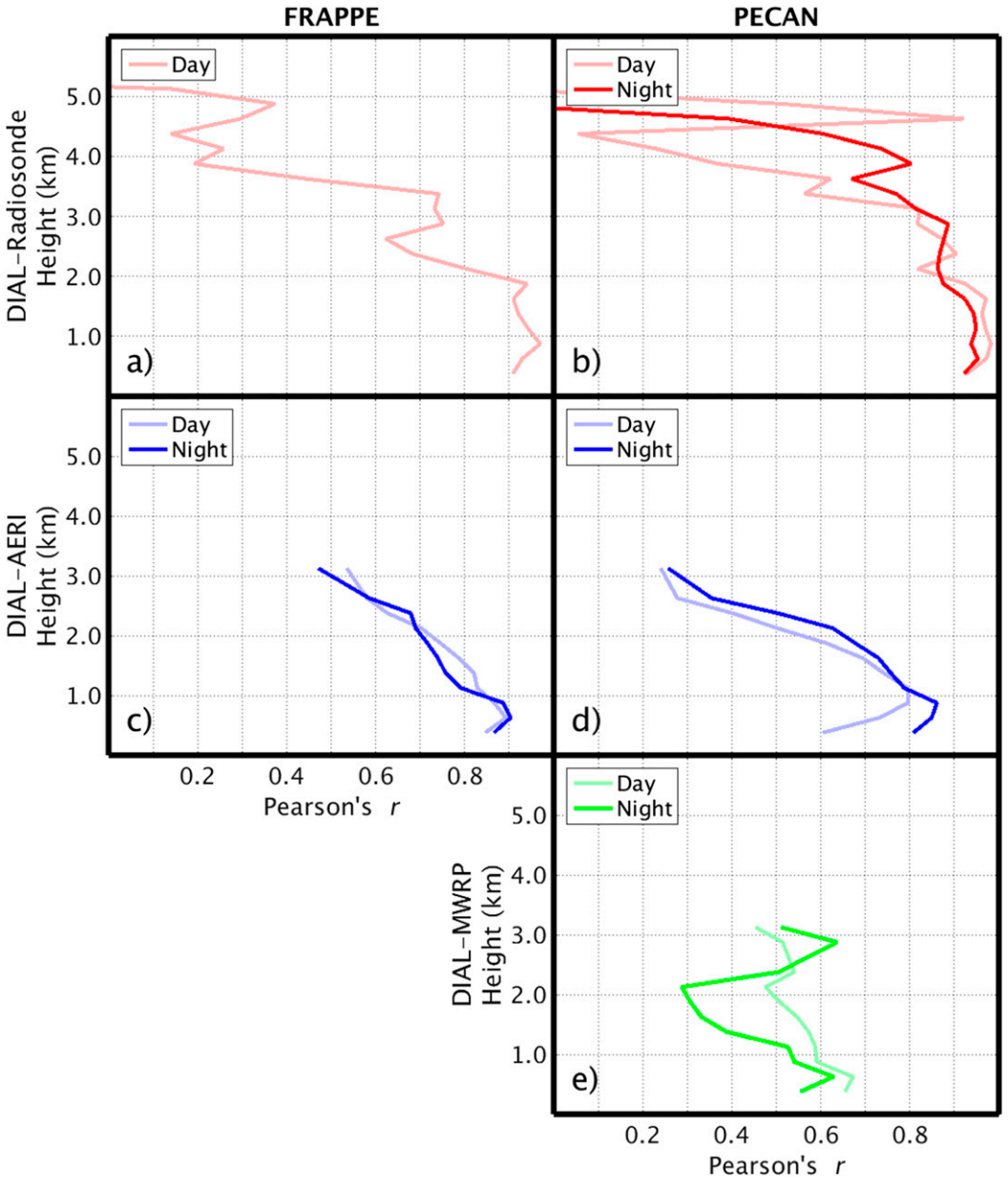

FIG. 5. Vertical profiles of Pearson's *r* for DIAL and (a),(b) radiosonde, (c),(d) AERI, and (e) MWRP absolute humidity comparisons for (left) FRAPPÉ and (right) PECAN. Daytime (nighttime) correlations are illustrated in light (dark) colors. (c)–(e) AERI and MWRP profiles are calculated only for DIAL profiles without elevated moist layers (see text for explanation).

radiosondes above 1.25 km. Strong agreement continues up to 3.5 km AGL, where the MPDs are <20% and the standard deviations are <50%. The PECAN comparisons between DIAL and radiosondes (Fig. 6b) similarly show very good agreement with MPDs < 10% and limited scatter (standard deviation < 50%) up to 2.75 km AGL. The PECAN MPDs are <22% up to 4.75 km AGL. The improved performance at PECAN is due to the numerous nighttime radiosonde launches with which to compare the DIAL profiles. The PECAN DIAL data exhibit a slight dry bias compared to radiosondes. Since this is not consistent with most of the other comparisons, the possibility of the RS41 radiosondes having a high moisture bias should be investigated. This will be discussed again in the subsequent section. All of the biases and standard deviations are quite large at higher altitudes (4–6 km AGL) due to the very low moisture content. This causes dramatic differences in

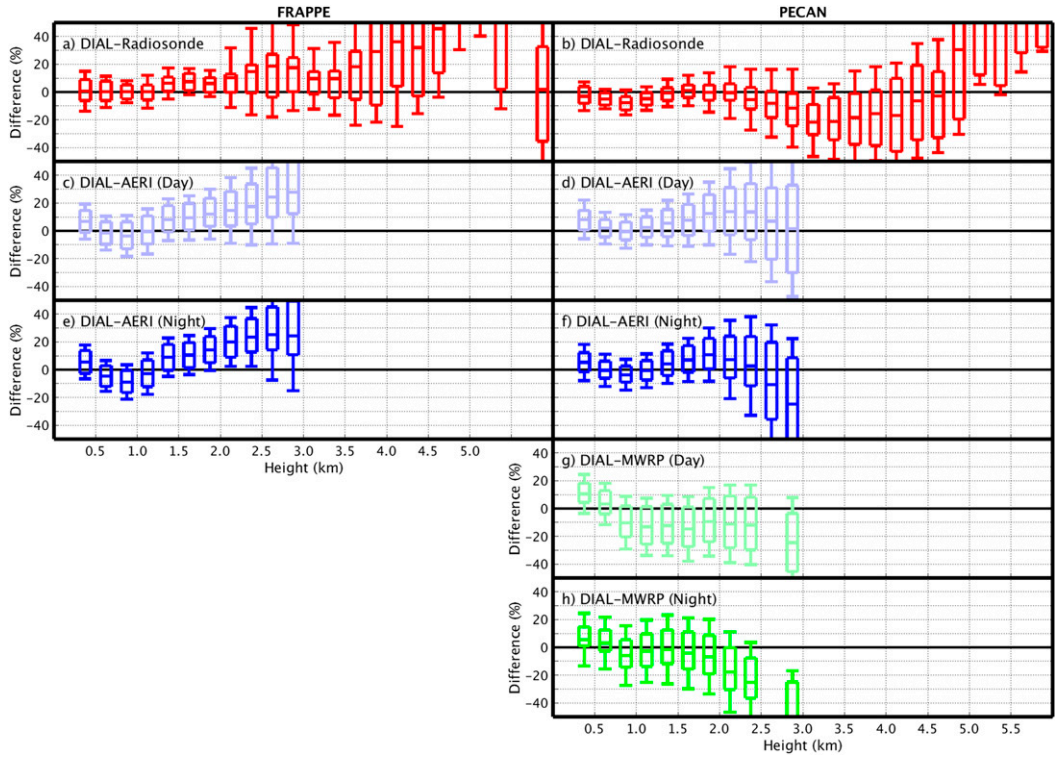

FIG. 6. Mean percentage difference (horizontal colored lines), 25%–75% range (boxes), and standard deviations (whiskers) for 250-m height bins from (a),(b) DIAL–radiosonde, (c)–(f) DIAL–AERI, and (g),(h) DIAL–MWRP comparisons from (left) FRAPPÉ and (right) PECAN. (c),(d),(g) Daytime and (e),(f),(h) nighttime comparisons are shown with the same color scheme as in Fig. 5. (c)–(e) AERI and MWRP profiles are calculated only for DIAL profiles without elevated moist layers (see text for explanation).

the statistical percentage comparisons. However, there is valuable and representative information content in the DIAL data up to at least 6 km. This will be further addressed when assessing longer averaging times in the upcoming PWV time series discussion.

The DIAL–AERI MPDs are <10% up to 1.75 km AGL both day and night for both campaigns (Figs. 6c–f). Furthermore, the MPDs in PECAN at night are <10% up to 2.75 km. The PECAN box plots illustrate greater MPD and greater variability above 1.75 km AGL than FRAPPÉ, likely caused by reduced AERI performance within the higher water vapor content of Kansas during PECAN than in Colorado during FRAPPÉ as described with Figs. 5c,d above. The AERI signal degrades with altitude, so the comparisons are shown only up to 3 km.

The PECAN box plots for DIAL–MWRP comparisons for day and night are shown in Figs. 6g,h, respectively. The MPDs are <10% at night up to 1 km AGL. The DIAL is drier than MWRP both day and night above 750 m. The agreement is best at night with <10% MPDs up to 1.75 km (Fig. 6h).

The highest-quality comparisons, in terms of MPDs and standard deviations, are obtained between the nighttime DIAL–radiosonde comparisons, illustrating excellent agreement up to 4.75 km. The nighttime DIAL–AERI comparisons show excellent agreement up to 2.75 km.

d. *Profile shape comparisons*

The modified Taylor plots (Fig. 7) allow for an objective description of the profile-to-profile agreement of the two datasets; a perfect agreement would have $r = 1$ and SDR = 1 (although this could still allow for a bias between the two instruments). These DIAL–radiosonde comparisons were made for both field campaigns between 300 m and 6 km AGL for day and night (Figs. 7a,b). Most of the points are clustered around the optimal result of r and SDR of 1. The majority of the points, in particular the 25%–75% range of points shown by the crosses, are near the optimal range. This gives further confidence for well-behaved DIAL profiles in that they are consistent with the standard radiosonde water vapor measurements from 300 m up to 6 km AGL. While the MPDs are relatively high above 3.75 km AGL for FRAPPÉ and above 4.75 km AGL for PECAN (Figs. 6a,b), there remains strong agreement between the DIAL and radiosonde

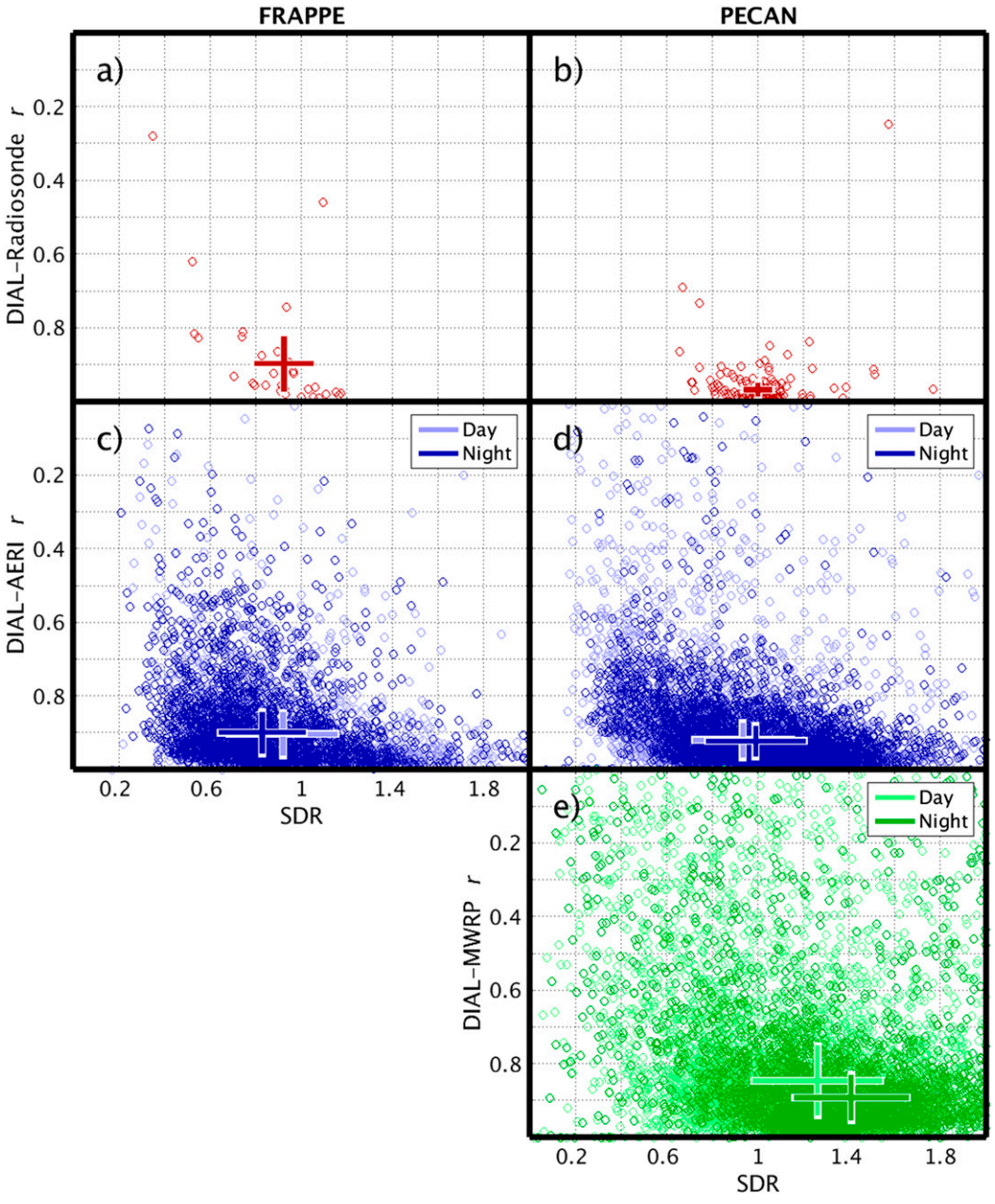

FIG. 7. Modified Taylor plot comparison of r vs SDR; see text for explanation. Comparisons are for (a),(b) DIAL–radiosonde compared for 300 m–6 km AGL, (c),(d) DIAL–AERI compared for 300 m–3 km AGL, and (e) DIAL–MWRP compared for 300 m–3 km AGL for (left) FRAPPÉ and (right) PECAN. Crosses represent 25th–75th percentile range of points with daytime comparisons shown in light colors and nighttime in dark colors. (c)–(e) AERI and MWRP comparisons are shown only for DIAL profiles without elevated moist layers (see text for explanation).

observations up to 6 km AGL. This point will be further illustrated in the next section.

For the more numerous data points of the DIAL–AERI comparisons from 300 m to 3 km, the bulk of the comparison profiles are concentrated near (1,1), particularly at night during PECAN, when the DIAL performance is optimal due to the high signal-to-noise ratio (Figs. 7c,d). The two campaigns have similar results, except that the nighttime cross is closer to (1,1) for PECAN compared with FRAPPÉ. There is substantially more variability in the DIAL–AERI points compared to the tight clustering of DIAL–radiosonde

points. This is due to a combination of 1) many more comparison profiles due to the continuously operating DIAL and AERI (see Table 2 for the number of profiles used in each comparison), 2) the difficulty in DIAL daytime measurements (due to the lower signal-to-noise ratio caused by the solar background) resulting in more scatter in the daytime comparisons, 3) the slight decrease in the information content of the AERI observations in the AERI retrievals during moist conditions of PECAN, and 4) the decrease in the vertical grid spacing of the passive AERI retrieval with altitude above the ground, whereas the DIAL grid spacing remains constant at 75 m.

The modified Taylor plot comparing DIAL with MWRP from 300 m to 3 km during PECAN is shown in Fig. 7e. The two datasets show agreement, but there is greater scatter than the DIAL–AERI comparisons (Figs. 7c,d). The increased scatter is due to the much lower information content of the MWRP moisture retrievals relative to the AERI (see Löhnert et al. 2009). The high SDRs suggest that the DIAL is measuring more variability in its profiles than does the MWRP. In summary, the relationships between these modified Taylor analyses show that the DIAL profiles are consistently similar with the radiosonde, AERI, and MWRP profiles.

e. Column-integrated PWV comparisons

Table 3 lists the 30-min-averaged GPS PWV, along with 30-min-averaged radiosonde, DIAL, and AERI PWV calculated over various height ranges. The time series are shown as 12-h-averaged PWV values to eliminate some of the noise in the 30-min data (Fig. 8). It is again apparent that Kansas is more moist than Colorado. Table 3 shows that FRAPPÉ exhibits 10.3 mm lower GPS PWV values (mean of 21.4 mm) compared to PECAN PWV values (mean of 31.7 mm). The GPS and radiosonde total column PWV measurements are consistently the highest values, and they generally agree with each other. They both measure the total column water vapor, while the other instruments provide height-limited data. The radiosonde PWV values are higher than the GPS values by 0.8 mm in FRAPPÉ and 2.1 mm in PECAN due to 1) potential cloud penetration biasing the radiosonde moisture measurements and 2) the fact that the radiosonde drifts horizontally upon ascent and is not measuring the same 10–15-km-wide vertical column as the GPS retrieval. Additionally, the larger moist bias observed by the RS41 radiosondes is consistent with the moist bias shown in comparison with the DIAL during PECAN (Fig. 6b). This suggestion of a possible RS41 moist bias during PECAN should be further investigated.

TABLE 3. Mean values of PWV measurements determined using 75-m spatial averaging for range-resolved instruments and 30-min temporal averaging for all.

Instrument (height range)	Mean (mm)
FRAPPÉ	
GPS (total column)	21.4
Radiosondes (variable: full ascent)	22.2
Radiosondes (0–3 km)	16.7
Radiosondes (0.3–3 km)	14.2
Radiosondes (0.3–6 km)	18.8
DIAL (0.3–3 km)	13.7
DIAL (0.3–6 km)	18.0
AERI (0–3 km)	16.9
AERI (0.3–3 km)	14.3
PECAN	
GPS (total column)	31.7
Radiosondes (variable: full ascent)	33.8
Radiosondes (0–3 km)	26.9
Radiosondes (0.3–3 km)	22.5
Radiosondes (0.3–6 km)	27.9
DIAL (0.3–3 km)	20.2
DIAL (0.3–6 km)	24.1
AERI (0–3 km)	25.3
AERI (0.3–3 km)	21.3

The remotely sensed PWV values derived from DIAL and AERI data track well, but they have clear and expected low biases compared with GPS PWV (Fig. 8). The AERI and DIAL traces averaged from 300 m to 3 km in altitude are similar to each because they are sampling the same height region, and they have previously been shown to compare well up to 3 km (see Figs. 4, 5). The DIAL measurements are 0.5–2.3 mm drier than AERI and radiosondes in the 0.3–3-km height interval (see Table 3). The DIAL and AERI traces are both substantially lower than the GPS PWV value due to their 0.3–3-km AGL limited height range with DIAL biases of 7.7 (11.5) mm in FRAPPÉ (PECAN). When AERI data are used from 0 to 3 km, the addition of the low-level moisture allows for more of the PWV to be recovered. The bias between the 0–3-km AERI and GPS PWV is 4.5 mm for FRAPPÉ and 6.4 mm for PECAN. Some of the bias is also recovered when the DIAL is integrated from 300 m to 6 km. The GPS–DIAL bias is then reduced to 3.4 mm for FRAPPÉ and 7.6 mm for PECAN, suggesting that the midlevel moisture is a significant contributor to the total column PWV. Figure 8 shows that the 0.3–6-km AGL DIAL trace more closely matches the GPS trace in FRAPPÉ, indicating higher midlevel moisture in Colorado than Kansas, likely due to the deeper BL in Colorado (cf. Figs. 1a,c). Even though the Pearson's r comparison between the DIAL and radiosondes is low for heights above 4.5 km (see Figs. 5a,b), the DIAL provides useful and reliable information about moisture content up to 6 km,

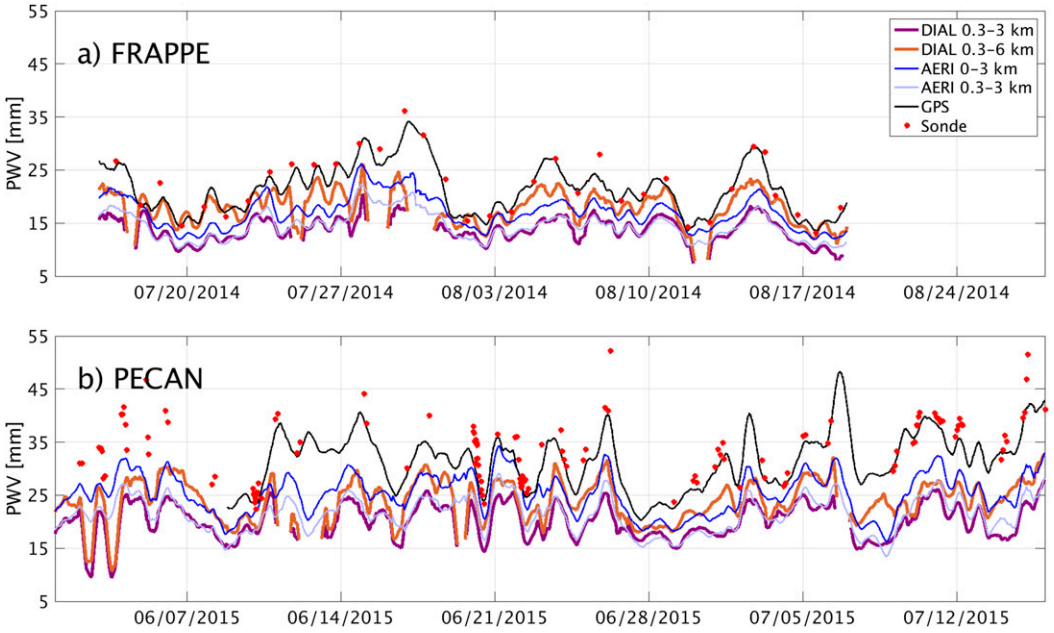

FIG. 8. Time series of 12-h-averaged PWV (mm) derived from GPS receivers (black lines) and calculated from radiosonde ascents (red dots), and from DIAL (thick purple lines: 0.3–3 km AGL; thick orange lines: 0.3–6 km AGL) and AERI (light blue lines: 0.3–3 km AGL; dark blue lines: 0–3 km AGL) profiles.

particularly when averaged over time periods longer than 5 min.

4. Summary and outlook

The new water vapor micropulse DIAL is proven to provide continuous water vapor profiles that are consistent with other instruments, including radiosondes, AERIs, MWRP, and GPS receivers as summarized in Table 4. The DIAL compares well with all instruments during both day and night and in both clear-sky and cloudy conditions (providing water vapor measurements up to cloud base). The Pearson's correlation coefficient between the DIAL and all radiosondes from 300 m to 3 km (300 m–6 km) is 0.92 (0.88) for FRAPPÉ, 0.97 (0.96) for PECAN, and 0.96 (0.95) for the combined dataset. The DIAL–radiosonde r is greater than 0.9 up to 2.0 km AGL, and is greater than 0.6 up to 3.5 km AGL during the day and up to 4.5 km AGL at night. The DIAL–AERI r is greater than 0.8 up to 1 km AGL and greater than 0.6 up to ~2 km AGL, where the AERI data are most reliable. Similarly, the best DIAL–MWRP comparisons are obtained below 1.5 km AGL. When there are no intervening clouds, the DIAL consistently provides accurate moisture measurements up to 3.5 km AGL during the daytime and up to 4.5 km AGL at night. It provides further accurate moisture information up to 6 km when averaged over time periods longer than 5 min, as evidenced in the comparisons with the GPS PWV.

One distinct advantage of the DIAL over radiosondes is its continuous operations. The benefits of the DIAL over AERI and MWRP are the uniform resolution from 300 m up to above the top of the BL and the unambiguous derivation of water vapor, which allows for the detection of elevated moist or dry layers. The DIAL

TABLE 4. Summary of comparisons and results.

Instrument	Resolution (time; range)	Averaging (time; height range)	Pearson's r (FRAPPÉ, PECAN, combined)
Radiosondes	1 s; 4–6 m	5 min; 0.3–3.0 km	0.92, 0.97, 0.96
Radiosondes	1 s; 4–6 m	5 min; 0.3–6.0 km	0.88, 0.96, 0.95
AERI, all profiles	5 min; 0.05–2.5 km	5 min; 0.3–3.0 km	0.86, 0.85, 0.85
AERI, similar profiles only	5 min; 0.05–2.5 km	5 min; 0.3–3.0 km	0.88, 0.90, 0.90
MWRP, all profiles	5 min; 0.05–0.25 km	5 min; 0.3–3.0 km	N/A, 0.71, 0.71
MWRP, similar profiles only	5 min; 0.05–0.25 km	5 min; 0.3–3.0 km	N/A, 0.71, 0.71
GPS receivers	30 min; total column	30 min; total column	0.40, 0.46, 0.44

advantage over GPS receivers is the range-resolved moisture measurements. The continuous unattended operations and high-quality water vapor profiles from the DIAL make it an appealing candidate system to function as part of a potential nationwide network of thermodynamic profiling instruments.

Numerous data analysis activities are underway using the DIAL data, including project-long characterization of the moisture content, depth, and horizontal and vertical advection. It is expected that this may be useful for better understanding and forecasting of convection initiation and evolution. Work is in progress to combine the DIAL profiles with high-resolution wind profiles from NCAR's 449-MHz wind profiler during PECAN to obtain vertical moisture flux profiles. Flux profiles were previously calculated using collocated DIAL and Doppler lidar or the radar–radio acoustic sounding system (RASS) by Senff et al. (1994), Wulfmeyer (1999), and Linné et al. (2007). A further application would be to utilize the DIAL's vertical water vapor variance estimates along with an ancillary surface flux measurement and the top-down and bottom-up diffusion concept (e.g., Wyngaard and Brost 1984; Moeng and Wyngaard 1984, 1989; Patton et al. 2003) to estimate water vapor fluxes and BL entrainment (e.g., Kiemle et al. 1997; Turner et al. 2014; Wulfmeyer et al. 2016). Further research is underway to utilize collocated DIAL profiles as an additional constraint to improve upon the AERI temperature profile retrievals.

Following PECAN, the DIAL pulse timing was adjusted and the lowest range gate is now 225 m. Operating the instrument with a shorter laser pulse duration would allow for a further reduction in the lowest range. For example, a 75-m lowest range gate should be possible if the pulse duration is cut in half—with the trade-off that there would be a reduced maximum range due to the reduced output power. The most recent version of the instrument—within a 2 m × 2 m × 1 m field enclosure—is integrated with a scientific-grade surface station to measure temperature, pressure, and relative humidity. The long-term objectives are to build a network of 10 water vapor DIALs to better characterize the horizontal moisture variability and to assess the DIAL's value in data assimilation for improving mesoscale forecast and QPF skill.

Acknowledgments. The FRAPPÉ and PECAN PIs and participants are gratefully acknowledged for bringing together such rich, diverse, and comprehensive datasets. The data are available via the online data archives (at http://www-air.larc.nasa.gov/missions/discover-aq/discover-aq.html and http://data.eol.ucar.edu/master_list/?project=PECAN, respectively). We are grateful to Rit Carbone (NCAR) for his thoughtful, consistent, and tireless support, which was essential for the DIAL development to succeed.

We thank the Cooperative Institute for Mesoscale Meteorological Studies at the University of Oklahoma for funding to help field the DIAL during PECAN. Thanks go to UW–Madison for collecting and sharing their FRAPPÉ AERI and radiosonde data. We are grateful to Rich Clark, Todd Sikora, and the Millersville University team of undergraduate students for collecting and sharing their PECAN/Ellis radiosonde dataset. We thank John Hanesiak, Kyle Ziolkowski, and Scott Kehler (U. Manitoba) for collecting and sharing their PECAN MWRP data. We thank the ARM program, and in particular Jon Gero, Denny Hackel, and Coda Phillips, for installing the AERI at the Ellis site for PECAN.

The insightful discussions with Holger Vömel (NCAR), Amin Nehrir (NASA), Jim Wilson (NCAR), and Volker Wulfmeyer (U. Hohenheim) are much appreciated. Thoughtful reviews by Ned Patton (NCAR), Matt Hayman (NCAR), and Jack Kain (NSSL) greatly improved the quality of earlier versions of this manuscript. Comments and suggestions from three anonymous reviewers improved the clarity and content of the manuscript.

Support of the second author (KW) through the NCAR Short-Term Explicit Prediction (STEP) program is greatly appreciated.

REFERENCES

Ansmann, A., and J. Bösenberg, 1987: Correction scheme for spectral broadening by Rayleigh scattering in differential absorption lidar measurements of water vapor in the troposphere. *Appl. Opt.*, **26**, 3026–3032, doi:10.1364/AO.26.003026.

Behrendt, A., and Coauthors, 2007: Intercomparison of water vapor data measured with lidar during IHOP_2002. Part I: Airborne to ground-based lidar systems and comparisons with chilled-mirror hygrometer radiosondes. *J. Atmos. Oceanic Technol.*, **24**, 3–21, doi:10.1175/JTECH1924.1.

——, V. Wulfmeyer, A. Riede, G. Wagner, S. Pal, H. Bauer, M. Radlach, and F. Späth, 2009: Three-dimensional observations of atmospheric humidity with a scanning differential absorption lidar. *Remote Sensing of Clouds and the Atmosphere XIV*, R. H. Picard et al., Eds., International Society for Optical Engineering (SPIE Proceedings, Vol. 7475), 74750L, doi:10.1117/12.835143.

Bevis, M., S. Businger, T. A. Herring, C. Rocken, R. A. Anthes, and R. H. Ware, 1992: GPS meteorology: Remote sensing of atmospheric water vapor using the global positioning system. *J. Geophys. Res.*, **97**, 15 787–15 801, doi:10.1029/92JD01517.

——, ——, ——, R. A. Anthes, C. Rocken, R. H. Ware, and S. R. Chiswell, 1994: GPS meteorology: Mapping zenith wet delays onto precipitable water. *J. Appl. Meteor.*, **33**, 379–387, doi:10.1175/1520-0450(1994)033<0379:GMMZWD>2.0.CO;2.

Bhawar, R., and Coauthors, 2011: The water vapour intercomparison effort in the framework of the Convective and Orographically-induced Precipitation Study: Airborne-to-ground-based and airborne-to-airborne lidar systems. *Quart. J. Roy. Meteor. Soc.*, **137**, 325–348, doi:10.1002/qj.697.

Blumberg, W. G., D. D. Turner, U. Löhnert, and S. Castleberry, 2015: Ground-based temperature and humidity profiling using spectral infrared and microwave observations. Part II: Actual retrieval performance in clear-sky and cloudy conditions. *J. Appl. Meteor. Climatol.*, **54**, 2305–2319, doi:10.1175/JAMC-D-15-0005.1.

Browell, E. V., and Coauthors, 1997: LASE validation experiment. *Advances in Atmospheric Remote Sensing with Lidar*, A. Ansmann et al., Eds., Springer Verlag, 289–295, doi:10.1007/978-3-642-60612-0_70.

Bruneau, D., P. Quaglia, C. Flamant, M. Meissonnier, and J. Pelon, 2001: Airborne lidar LEANDRE II for water-vapor profiling in the troposphere. I. System description. *Appl. Opt.*, **40**, 3450–3475, doi:10.1364/AO.40.003450.

Businger, S., and Coauthors, 1996: The promise of GPS in atmospheric monitoring. *Bull. Amer. Meteor. Soc.*, **77**, 5–18, doi:10.1175/1520-0477(1996)077<0005:TPOGIA>2.0.CO;2.

Cadeddu, M. P., J. C. Liljegren, and D. D. Turner, 2013: The Atmospheric Radiation Measurement (ARM) Program network of microwave radiometers: Instrumentation, data and retrievals. *Atmos. Meas. Tech.*, **6**, 2359–2372, doi:10.5194/amt-6-2359-2013.

Cimini, D., T. J. Hewison, L. Martin, J. Güldner, C. Gafford, and F. Marzano, 2006: Temperature and humidity profile retrievals from ground-based radiometers during TUC. *Meteor. Z.*, **15**, 45–56, doi:10.1127/0941-2948/2006/0099.

——, and Coauthors, 2012: An international network of ground-based microwave radiometers for the assimilation of temperature and humidity profiles into NWP models. *Proc. Ninth Int. Symp. on Tropospheric Profiling*, European Space Agency, L'Aquila, Italy, P45. [Available online at http://cetemps.aquila.infn.it/istp/proceedings/Session_P_Posters/P45_Cimini.pdf.]

Clark, R., 2016: FP3 Ellis, KS radiosonde data, version. 2.0. UCAR/NCAR Earth Observing Laboratory, accessed 29 January 2016, doi:10.5065/D6GM85DZ.

Crewell, S., and Coauthors, 2004: The BALTEX Bridge Campaign: An integrated approach for a better understanding of clouds. *Bull. Amer. Meteor. Soc.*, **85**, 1565–1584, doi:10.1175/BAMS-85-10-1565.

Crook, N. A., 1996: Sensitivity of moist convection forced by boundary layer processes to low-level thermodynamic fields. *Mon. Wea. Rev.*, **124**, 1767–1785, doi:10.1175/1520-0493(1996)124<1767:SOMCFB>2.0.CO;2.

Dinoev, T., V. Simeonov, Y. Arshinov, S. Bobrovnikov, P. Ristori, B. Calpini, M. Parlange, and H. van den Bergh, 2013: Raman lidar for meteorological observations, RALMO—Part 1: Instrument description. *Atmos. Meas. Tech.*, **6**, 1329–1346, doi:10.5194/amt-6-1329-2013.

Ehret, G., C. Kiemle, W. Renger, and G. Simmet, 1993: Airborne remote sensing of tropospheric water vapor with a near-infrared differential absorption lidar system. *Appl. Opt.*, **32**, 4534–4551, doi:10.1364/AO.32.004534.

Flocke, F., and Coauthors, 2015: The Front Range Air Pollution and Photochemistry Experiment (FRAPPÉ)—An overview. *2015 Fall Meeting*, San Francisco, CA, Amer. Geophys. Union, Abstract A12A-01.

Geerts, B., and Coauthors, 2016: The 2015 Plains Elevated Convection at Night (PECAN) field project. *Bull. Amer. Meteor. Soc.*, doi:10.1175/BAMS-D-15-00257.1, in press.

Goldsmith, J. E. M., F. H. Blair, S. E. Bisson, and D. D. Turner, 1998: Turn-key Raman lidar for profiling atmospheric water vapor, clouds, and aerosols. *Appl. Opt.*, **37**, 4979–4990, doi:10.1364/AO.37.004979.

Hanesiak, J., and D. Turner, 2015: FP3 University of Manitoba MWR radiometrics retrieval profile data, version 1.0. UCAR/NCAR Earth Observing Laboratory, accessed 21 August 2015, doi:10.5065/D6KH0KCB.

Harnisch, F., M. Weissman, C. Cardinali, and M. Wirth, 2011: Experimental assimilation of DIAL water vapour observations in the ECMWF global model. *Quart. J. Roy. Meteor. Soc.*, **137**, 1532–1546, doi:10.1002/qj.851.

Hartung, D. C., J. A. Otkin, R. A. Petersen, D. D. Turner, and W. F. Feltz, 2011: Assimilation of surface-based boundary layer profiler observations during a cool-season weather event using an observing system simulation experiment. Part II: Forecast assessment. *Mon. Wea. Rev.*, **139**, 2327–2346, doi:10.1175/2011MWR3623.1.

Hayman, M., S. Spuler, B. Morley, and E. Eloranta, 2015: Design of a low cost diode-laser-based High Spectral Resolution Lidar (HSRL). *Proc. 27th Int. Laser Radar Conf.*, New York, NY, NOAA CREST, 06006. [Available online at http://www.epj-conferences.org/articles/epjconf/pdf/2016/14/epjconf_ilrc2016_06006.pdf.]

Hewison, T., 2007: 1D-VAR retrievals of temperature and humidity profiles from a ground-based microwave radiometer. *IEEE Trans. Geosci. Remote Sens.*, **45**, 2163–2168, doi:10.1109/TGRS.2007.898091.

Illingworth, A. J., D. Cimini, C. Gaffard, M. Haeffelin, V. Lehmann, U. Löhnert, E. J. O'Connor, and D. Ruffieux, 2015: Exploiting existing ground-based remote sensing networks to improve high-resolution weather forecasts. *Bull. Amer. Meteor. Soc.*, **96**, 2107–2125, doi:10.1175/BAMS-D-13-00283.1.

Ismail, S., and E. V. Browell, 1989: Airborne and spaceborne lidar measurements of water vapor profiles: A sensitivity analysis. *Appl. Opt.*, **28**, 3603–3615, doi:10.1364/AO.28.003603.

Kiemle, C., G. Ehret, A. Giez, K. J. Davis, D. H. Lenschow, and S. P. Oncley, 1997: Estimation of boundary layer humidity fluxes and statistics from airborne differential absorption lidar (DIAL). *J. Geophys. Res.*, **102**, 29 189–29 203, doi:10.1029/97JD01112.

Knuteson, R. O., and Coauthors, 2004a: The Atmospheric Emitted Radiance Interferometer. Part I: Instrument design. *J. Atmos. Oceanic Technol.*, **21**, 1763–1776, doi:10.1175/JTECH-1662.1.

——, and Coauthors, 2004b: The Atmospheric Emitted Radiance Interferometer. Part II: Instrument performance. *J. Atmos. Oceanic Technol.*, **21**, 1777–1789, doi:10.1175/JTECH-1663.1.

Küchler, N., D. D. Turner, U. Löhnert, and S. Crewell, 2016: Calibrating ground-based microwave radiometers: Uncertainty and drifts. *Radio Sci.*, **51**, 311–327, doi:10.1002/2015RS005826.

Liljegren, J. C., 2004: Improved retrievals of temperature and water vapor profiles with a twelve-channel radiometer. *Eighth Symp. on Integrated Observing and Assimilation Systems for Atmosphere, Oceans, and Land Surface (IOAS-AOLS)*, Seattle, WA, Amer. Meteor. Soc., 4.7. [Available online at https://ams.confex.com/ams/84Annual/techprogram/paper_69734.htm.]

Lin, P.-F., P.-L. Chang, B. J.-D. Jou, J. W. Wilson, and R. D. Roberts, 2011: Warm season afternoon thunderstorm characteristics under weak synoptic-scale forcing over Taiwan Island. *Wea. Forecasting*, **26**, 44–60, doi:10.1175/2010WAF2222386.1.

Linné, H., B. Hennemuth, J. Bösenberg, and K. Ertel, 2007: Water vapour flux profiles in the convective boundary layer. *Theor. Appl. Climatol.*, **87**, 201–211, doi:10.1007/s00704-005-0191-7.

Löhnert, U., and O. Maier, 2012: Operational profiling of temperature using ground-based microwave radiometry at Payerne: Prospects and challenges. *Atmos. Meas. Tech.*, **5**, 1121–1134, doi:10.5194/amt-5-1121-2012.

——, D. D. Turner, and S. Crewell, 2009: Ground-based temperature and humidity profiling using spectral infrared and microwave observations. Part I: Simulated retrieval performance in clear-sky conditions. *J. Appl. Meteor. Climatol.*, **48**, 1017–1032, doi:10.1175/2008JAMC2060.1.

Machol, J. L., and Coauthors, 2004: Preliminary measurements with an automated compact differential absorption lidar for the profiling of water vapor. *Appl. Opt.*, **43**, 3110–3121, doi:10.1364/AO.43.003110.

Maschwitz, G., U. Löhnert, S. Crewell, T. Rose, and D. D. Turner, 2013: Investigation of ground-based microwave radiometer calibration techniques at 530 hPa. *Atmos. Meas. Tech.*, **6**, 2641–2658, doi:10.5194/amt-6-2641-2013.

Moeng, C.-H., and J. C. Wyngaard, 1984: Statistics of conservative scalars in the convective boundary layer. *J. Atmos. Sci.*, **41**, 3161–3169, doi:10.1175/1520-0469(1984)041<3161:SOCSIT>2.0.CO;2.

——, and ——, 1989: Evaluation of turbulent transport and dissipation closures in second-order modeling. *J. Atmos. Sci.*, **46**, 2311–2330, doi:10.1175/1520-0469(1989)046<2311:EOTTAD>2.0.CO;2.

Moore, A. W., and Coauthors, 2015: National Weather Service forecasters use GPS precipitable water vapor for enhanced situational awareness during the Southern California summer monsoon. *Bull. Amer. Meteor. Soc.*, **96**, 1867–1877, doi:10.1175/BAMS-D-14-00095.1.

NRC, 2009: *Observing Weather and Climate from the Ground Up: A Nationwide Network of Networks.* National Academies Press, 250 pp., doi:10.17226/12540.

——, 2010: *When Weather Matters: Science and Service to Meet Critical Societal Needs*. National Academies Press, 198 pp., doi:10.17226/12888.

——, 2012: *Weather Services for the Nation: Becoming Second to None*. National Academies Press, 86 pp., doi:10.17226/13429.

Nehrir, A. R., 2011: Development of an eye-safe diode-laser-based micro-pulse differential absorption lidar (MP-DIAL) for atmospheric water-vapor and aerosol studies. Ph.D. thesis, Montana State University, 270 pp.

——, K. S. Repasky, J. L. Carlsten, M. D. Obland, and J. A. Shaw, 2009: Water vapor profiling using a widely tunable, amplified diode-laser-based differential absorption lidar (DIAL). *J. Atmos. Oceanic Technol.*, **26**, 733–745, doi:10.1175/2008JTECHA1201.1.

——, ——, and ——, 2011: Eye-safe diode-laser-based micropulse differential absorption lidar (DIAL) for water vapor profiling in the lower troposphere. *J. Atmos. Oceanic Technol.*, **28**, 131–147, doi:10.1175/2010JTECHA1452.1.

——, ——, and ——, 2012: Micropulse water vapor differential absorption lidar: Transmitter design and performance. *Opt. Express*, **20**, 25 137–25 151, doi:10.1364/OE.20.025137.

Otkin, J. A., D. C. Hartung, D. D. Turner, R. A. Petersen, W. F. Feltz, and E. Janzon, 2011: Assimilation of surface-based boundary layer profiler observations during a cool-season weather event using an observing system simulation experiment. Part I: Analysis impact. *Mon. Wea. Rev.*, **139**, 2309–2326, doi:10.1175/2011MWR3622.1.

Paine, S. N., D. D. Turner, and N. Küchler, 2014: Understanding thermal drift in liquid nitrogen loads used for radiometric calibration in the field. *J. Atmos. Oceanic Technol.*, **31**, 647–655, doi:10.1175/JTECH-D-13-00171.1.

Patton, E. G., P. P. Sullivan, and K. J. Davis, 2003: The influence of a forest canopy on top-down and bottom-up diffusion in the planetary boundary layer. *Quart. J. Roy. Meteor. Soc.*, **129**, 1415–1434, doi:10.1256/qj.01.175.

Poberaj, G., A. Fix, A. Assion, M. Wirth, C. Kiemle, and G. Ehret, 2002: Airborne all-solid-state DIAL for water vapour measurements in the tropopause region: System description and assessment of accuracy. *Appl. Phys.*, **75B**, 165–172, doi:10.1007/s00340-002-0965-x.

Reichardt, J., U. Wandinger, V. Klein, I. Mattis, B. Hilber, and R. Begbie, 2012: RAMSES: German Meteorological Service autonomous Raman lidar for water vapor, temperature, aerosol, and cloud measurements. *Appl. Opt.*, **51**, 8111–8131, doi:10.1364/AO.51.008111.

Repasky, K., D. Moen, S. Spuler, A. Nehrir, and J. Carlsten, 2013: Progress towards an autonomous field deployable diode-laser-based differential absorption lidar (DIAL) for profiling water vapor in the lower troposphere. *Remote Sens.*, **5**, 6241–6259, doi:10.3390/rs5126241.

Senff, C., J. Bösenberg, and G. Peters, 1994: Measurement of water vapor flux profiles in the convective boundary layer with lidar and radar–RASS. *J. Atmos. Oceanic Technol.*, **11**, 85–93, doi:10.1175/1520-0426(1994)011<0085:MOWVFP>2.0.CO;2.

Solheim, F., J. Godwin, E. Westwater, Y. Han, S. Keihm, K. Marsh, and R. Ware, 1998: Radiometric profiling of temperature, water vapor, and cloud liquid water using various inversion methods. *Radio Sci.*, **33**, 393–404, doi:10.1029/97RS03656.

Späth, F., A. Behrendt, S. Kumar Muppa, S. Metzendorf, A. Riede, and V. Wulfmeyer, 2016: 3-D water vapor field in the atmospheric boundary layer observed with scanning differential absorption lidar. *Atmos. Meas. Tech.*, **9**, 1701–1720, doi:10.5194/amt-9-1701-2016.

Spuler, S. M., K. S. Repasky, B. Morley, D. Moen, M. Hayman, and A. R. Nehrir, 2015: Field-deployable diode-laser-based differential absorption lidar (DIAL) for profiling water vapor. *Atmos. Meas. Tech.*, **8**, 1073–1087, doi:10.5194/amt-8-1073-2015.

Stokes, G. M., and S. E. Schwartz, 1994: The Atmospheric Radiation Measurement (ARM) Program: Programmatic background and design of the Cloud and Radiation Test Bed. *Bull. Amer. Meteor. Soc.*, **75**, 1201–1221, doi:10.1175/1520-0477(1994)075<1201:TARMPP>2.0.CO;2.

Taylor, K. E., 2001: Summarizing multiple aspects of model performance in a single diagram. *J. Geophys. Res.*, **106**, 7183–7192, doi:10.1029/2000JD900719.

Turner, D. D., 2015: FP3 AERIoe thermodynamic profile retrieval data, version 1.0. UCAR/NCAR Earth Observing Laboratory, accessed 25 April 2016, doi:10.5065/D6Z31WV0.

——, and J. E. M. Goldsmith, 1999: Twenty-four-hour Raman lidar water vapor measurements during the Atmospheric Radiation Measurement Program's 1996 and 1997 water vapor intensive observation periods. *J. Atmos. Oceanic Technol.*, **16**, 1062–1076, doi:10.1175/1520-0426(1999)016<1062:TFHRLW>2.0.CO;2.

——, and U. Löhnert, 2014: Information content and uncertainties in thermodynamic profiles and liquid cloud properties retrieved from the ground-based Atmospheric Emitted Radiance Interferometer (AERI). *J. Appl. Meteor. Climatol.*, **53**, 752–771, doi:10.1175/JAMC-D-13-0126.1.

——, and R. G. Ellingson, Eds., 2016: *The Atmospheric Radiation Measurement (ARM) Program: The First 20 Years*. *Meteor. Monogr.*, No. 57, Amer. Meteor. Soc.

——, R. O. Knuteson, H. E. Revercomb, C. Lo, and R. G. Dedecker, 2006: Noise reduction of Atmospheric Emitted Radiance Interferometer (AERI) observations using principal component analysis. *J. Atmos. Oceanic Technol.*, **23**, 1223–1238, doi:10.1175/JTECH1906.1.

——, V. Wulfmeyer, L. K. Berg, and J. H. Schween, 2014: Water vapor turbulence profiles in stationary continental convective mixed layers. *J. Geophys. Res. Atmos.*, **119**, 11 151–11 165, doi:10.1002/2014JD022202.

——, J. E. M. Goldsmith, and R. A. Ferrare, 2016a: Development and applications of the ARM Raman lidar. *The Atmospheric Radiation Measurement Program: The First 20 Years*, *Meteor. Monogr.*, No. 57, Amer. Meteor. Soc., 18-1–18.15, doi:10.1175/AMSMONOGRAPHS-D-15-0016.1.

——, E. J. Mlawer, and H. E. Revercomb, 2016b: Water vapor observations in the ARM Program. *The Atmospheric Radiation Measurement (ARM) Program: The First 20 Years*, *Meteor. Monogr.*, No. 57, Amer. Meteor. Soc., 13.1–13.18, doi:10.1175/AMSMONOGRAPHS-D-15-0025.1.

UCAR/NCAR EOL, 2016a: FP3 NCAR/EOL water vapor DIAL, QC data in netCDF, version 2.0. UCAR/NCAR Earth Observing Laboratory, accessed 29 April 2016, doi:10.5065/D6SJ1HR1.

——, 2016b: NCAR/EOL water vapor DIAL, QC data in netCDF, version 1.0. UCAR/NCAR Earth Observing Laboratory, accessed 29 April 2016, doi:10.5065/D65B00NF.

Van Baelen, J., M. Reverdy, F. Tridon, L. Labbouz, G. Dick, M. Bender, and M. Hagen, 2011: On the relationship between water vapour field evolution and the life cycle of precipitation systems. *Quart. J. Roy. Meteor. Soc.*, **137**, 204–223, doi:10.1002/qj.785.

Vogelmann, H., and T. Trickl, 2008: Wide-range sounding of free-tropospheric water vapor with a differential-absorption lidar (DIAL) at a high altitude station. *Appl. Opt.*, **47**, 2116–2132, doi:10.1364/AO.47.002116.

Wagner, G., V. Wulfmeyer, F. Späth, A. Behrendt, and M. Schiller, 2013: High-power Ti:sapphire laser at 820 nm for scanning ground-based water–vapor differential absorption lidar. *Appl. Opt.*, **52**, 2454–2469, doi:10.1364/AO.52.002454.

Wang, J., L. Zhang, A. Dai, F. Immler, M. Sommer, and H. Vömel, 2013: Radiation dry bias correction of Vaisala RS92 humidity data and its impacts on historical radiosonde data. *J. Atmos. Oceanic Technol.*, **30**, 197–214, doi:10.1175/JTECH-D-12-00113.1.

Weckwerth, T. M., 2000: The effect of small-scale moisture variability on thunderstorm initiation. *Mon. Wea. Rev.*, **128**, 4017–4030, doi:10.1175/1520-0493(2000)129<4017:TEOSSM>2.0.CO;2.

——, J. W. Wilson, and R. M. Wakimoto, 1996: Thermodynamic variability within the convective boundary layer due to horizontal convective rolls. *Mon. Wea. Rev.*, **124**, 769–784, doi:10.1175/1520-0493(1996)124<0769:TVWTCB>2.0.CO;2.

——, V. Wulfmeyer, R. M. Wakimoto, R. M. Hardesty, J. W. Wilson, and R. M. Banta, 1999: NCAR–NOAA Lower-Tropospheric Water Vapor Workshop. *Bull. Amer. Meteor. Soc.*, **80**, 2339–2357, doi:10.1175/1520-0477(1999)080<2339:NNLTWV>2.0.CO;2.

——, L. J. Bennett, L. J. Miller, J. Van Baelen, P. Di Girolamo, A. M. Blyth, and T. J. Hertneky, 2014: An observational and modeling study of the processes leading to deep, moist convection in complex terrain. *Mon. Wea. Rev.*, **142**, 2687–2708, doi:10.1175/MWR-D-13-00216.1.

Wulfmeyer, V., 1999: Investigation of turbulent processes in the lower troposphere with water vapor DIAL and radar–RASS. *J. Atmos. Sci.*, **56**, 1055–1076, doi:10.1175/1520-0469(1999)056<1055:IOTPIT>2.0.CO;2.

——, and J. Bösenberg, 1998: Ground-based differential absorption lidar for water-vapor profiling: Assessment of accuracy, resolution and meteorological applications. *Appl. Opt.*, **37**, 3825–3844, doi:10.1364/AO.37.003825.

——, and C. Walther, 2001a: Future performance of ground-based and airborne water-vapor differential absorption lidar. I: Overview and theory. *Appl. Opt.*, **40**, 5304–5320, doi:10.1364/AO.40.005304.

——, and ——, 2001b: Future performance of ground-based and airborne water-vapor differential absorption lidar. II: Simulations of the precision of a near-infrared, high-power system. *Appl. Opt.*, **40**, 5321–5336, doi:10.1364/AO.40.005321.

——, H.-S. Bauer, M. Grzeschik, A. Behrendt, F. Vandenberghe, E. V. Browell, S. Ismail, and R. A. Ferrare, 2006: Four-dimensional variational assimilation of water vapor differential absorption lidar data: The first case study within IHOP_2002. *Mon. Wea. Rev.*, **134**, 209–230, doi:10.1175/MWR3070.1.

——, and Coauthors, 2015: A review of the remote sensing of lower tropospheric thermodynamic profiles and its indispensible role for understanding and simulation of water and energy cycles. *Rev. Geophys.*, **53**, 819–895, doi:10.1002/2014RG000476.

——, S. Kumar Muppa, A. Behrendt, E. Hammann, F. Späth, Z. Sorbjan, D. D. Turner, and R. M. Hardesty, 2016: Determination of convective boundary layer entrainment fluxes, dissipation rates, and the molecular destruction of variances: Theoretical description and a strategy for its confirmation with a novel lidar system synergy. *J. Atmos. Sci.*, **73**, 667–692, doi:10.1175/JAS-D-14-0392.1.

Wyngaard, J. C., and R. A. Brost, 1984: Top-down and bottom-up diffusion of a scalar in the convective boundary layer. *J. Atmos. Sci.*, **41**, 102–112, doi:10.1175/1520-0469(1984)041<0102:TDABUD>2.0.CO;2.